Basin Research

EAGE

Basin Research (2010) **22**, 249–269, doi: 10.1111/j.1365-2117.2009.00412.x

Late Cenozoic structural and stratigraphic evolution of the northern Chinese Tian Shan foreland

Honghua Lu,*† Douglas W. Burbank,† Youli Li* and Yunming Liu‡

*College of Urban and Environmental Sciences, Peking University, Beijing, PR China
†Institute for Crustal Studies, University of California at Santa Barbara, California, USA
‡School of Geographical Sciences, Southwest University, Chongqing, PR China

ABSTRACT

Three successive zones of fault-related folds disrupt the proximal part of the northern Tian Shan foreland in NW China. A new magnetostratigraphy of the Taxi He section on the north limb of the Tugulu anticline in the middle deformed zone clarifies the chronology of both tectonic deformation and depositional evolution of this collisional mountain belt. Our ~1200-m-thick section encompasses the upper Cenozoic terrigenous sequence within which ~300 sampling horizons yield an age span of ~8–2 Ma. Although the basal age in the Taxi He section of the Xiyu conglomerate (often cited as an indicator of initial deformation) is ~2.1 Ma, much earlier growth of the Tugulu anticline is inferred from growth strata dated at ~6.0 Ma. Folding of Neogene strata and angular unconformities in anticlines in the more proximal and distal deformed zones indicate deformation during Miocene and Early Pleistocene times, respectively. In the Taxi He area, sediment-accumulation rates significantly accelerate at ~4 Ma, apparently in response to encroaching thrust loads. Together, growth strata, angular unconformities, and sediment-accumulation rates document the northward migration of tectonic deformation into the northern Tian Shan foreland basin during the late Cenozoic. A progradational alluvial–lacustrine system associated with this northward progression is subdivided into two facies associations at Tugulu: a shallow lacustrine environment before ~5.9 Ma and an alluvial fan environment subsequently. The lithofacies progradation encompasses the time-transgressive Xiyu conglomerate deposits, which should only be recognized as a lithostratigraphic unit. Along the length of the foreland, the locus of maximum shortening shifts between the medial and proximal zones of folding, whereas the total shortening across the foreland remains quite homogeneous along strike, suggesting spatially steady tectonic forcing since late Miocene times.

INTRODUCTION

The Cenozoic India–Asia collision (Molnar & Tapponnier, 1975; Gansser, 1981; Molnar *et al.*, 1993; Tapponnier *et al.*, 2001) has significantly impacted the tectonic and climatic environment of high Asia. Exceptional topographic relief and the thick Cenozoic terrigenous sequences that have been shed into foreland basins provide an opportunity to probe the history of tectonic deformation related to this collision and to understand the tectonic and/or climatic controls on syndepositional systems.

Separating the Tarim Basin to the south from the Junggar Basin to the north, the east–west trending Tian Shan lies about 2000 km north of the initial India–Asia collision front (Deng *et al.*, 2000; Charreau *et al.*, 2005). Thick upper Cenozoic terrigenous sequences were deposited in the intramontane and foreland basins of the Tian Shan (e.g. Burbank *et al.*, 1999; Bullen *et al.*, 2001; Sun *et al.*, 2004; Charreau *et al.*, 2005, 2006; Chen *et al.*, 2007; Heermance *et al.*, 2007). Whereas the scarcity of faunal or floral fossils has provided only limited biostratigraphic age constraints on foreland strata, magnetostratigraphy has been successfully used to calibrate the terrestrial depositional record in this region (e.g. Zheng *et al.*, 2000; Chen *et al.*, 2002, 2007; Sun *et al.*, 2004, 2005a, b, 2007; Charreau *et al.*, 2005, 2006, 2008b; Huang *et al.*, 2006; Heermance *et al.*, 2007), despite some inherent uncertainties whenever dating sedimentary strata (Talling & Burbank, 1993). Many previous studies have focused on the timing of tectonic growth of the Tian Shan using combinations of geologic and geodetic data (e.g. Hendrix *et al.*, 1992; Avouac & Tapponnier, 1993; Avouac *et al.*, 1993; Abdrakhmatov *et al.*, 1996; Métivier & Gaudemer, 1997; Yang & Liu, 2002; Fu *et al.*, 2003), thermochronology (e.g. Hendrix *et al.*, 1994; Dumitru *et al.*, 2001; Bullen *et al.*, 2003; Sobel *et al.*, 2006), or magnetostratigraphy (e.g. Sun *et al.*, 2004; Charreau *et al.*, 2005, 2006; Huang *et al.*, 2006). In contrast, relatively few studies (Bullen *et al.*, 2001; Chen *et al.*, 2002, 2007; Heermance *et al.*, 2007) have focused on sedimentary facies in a robust temporal framework in order to delineate the depositional

Correspondence: Honghua Lu, Rm. 516, Ocean Building, Tongji University, Shanghai 200092, PR China. E-mail: lvhh2008@163.com

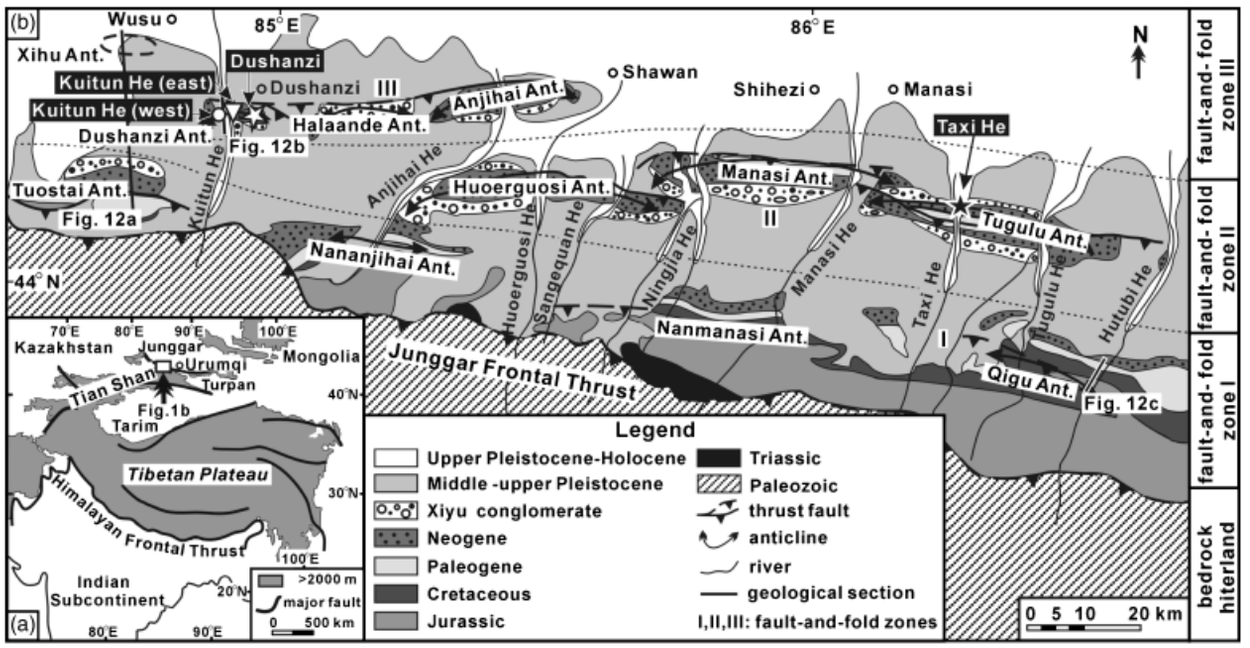

Fig. 1. (a) Overall geological setting in Central Asia (after Hendrix *et al.*, 1994). (b) Geological map of fault-and-fold zones I–III in the north margin of the Tian Shan (modified from Zhang *et al.*, 1994; Deng *et al.*, 2000), showing the tectonic setting and the Phanerozoic strata. Solid star indicates the paleomagnetic sampling site in this study at Taxi He. Open circle, triangle and star show the locations of the Kuitun He (west) section (Sun *et al.*, 2007), the Kuitun He (east) section (Charreau *et al.*, 2005) and the Dushanzi section (Sun *et al.*, 2004), respectively.

evolution of the upper Cenozoic coarsening-upward terrigenous sequences in the Tian Shan.

Based on a magnetostratigraphic study, Sun *et al.* (2004) concluded that thick conglomerate deposits were direct indicators of tectonic uplift in the Tian Shan. Others contend that, although changes in lithofacies and accumulation rates could indicate nearby tectonic deformation (Zheng *et al.*, 2000; Charreau *et al.*, 2005; Sun *et al.*, 2005b; Huang *et al.*, 2006), analogous changes could be driven by nontectonic forcing, including variations in climate (Molnar, 2001, 2004; Zhang *et al.*, 2001; Dupont-Nivet *et al.*, 2007), lithologic resistance in the source area, or transport distance (DeCelles & Giles, 1996; DeCelles *et al.*, 1998; Chen *et al.*, 2002; Charreau *et al.*, 2006; Heermance *et al.*, 2007) with the last variable being especially important in settings where tectonic deformation migrated in steps toward the foreland basin. Furthermore, lithofacies changes, such as the onset of conglomeratic deposition at any single location within a basin, commonly include a time lag from causative events in the hinterland (Jordan *et al.*, 1988; Jones *et al.*, 2004) or may only indicate local structural influences, rather than range-wide changes (Heermance *et al.*, 2007). Thus, tectonic interpretations of conglomeratic facies are best made in a reliable, three-dimensional, temporally controlled, depositional framework (Chen *et al.*, 2002, 2007; Heermance *et al.*, 2007). Such contexts illuminate patterns of time-transgressive facies migration and help restrain the tendency to treat facies in any given section as chronostratigraphic units (e.g. Li *et al.*, 1979; Huang & Cheng, 1981; Liu *et al.*, 1996).

Consequently, in order to improve understanding of the deformational history and of possible controls on deposition in the northern Tian Shan foreland, we completed a magnetostratigraphic study of a ~1200-m-thick, upper Cenozoic terrigenous sequence of foreland strata on the north limb of the Tugulu anticline in the middle fold-and-fault zone of the foreland (Fig. 1). Our paleomagnetic investigations provide a robust temporal framework spanning from ~8 to ~2 Ma within which we analyze sedimentary facies and discuss the controls of tectonic deformation on depositional evolution along the northern piedmont of the Chinese Tian Shan.

GEOLOGICAL SETTING AND STRATIGRAPHY

The ancestral Tian Shan was formed during the Permian after experiencing two Paleozoic accretion events within paleo-Asia (Windley *et al.*, 1990; Allen *et al.*, 1993; Carroll *et al.*, 1995; Sobel *et al.*, 2006): one along the southern margin of the range (Late Devonian–Early Carboniferous), which resulted in the accretion of the Tarim block onto the central Tian Shan; and the other along the northern margin (Late Carboniferous–Early Permian), which led to the amalgamation of the northern Tian Shan with the combined Tarim-central Tian Shan continental block. The subsequent Mesozoic deformation of the Tian Shan is characterized by three distinguishable episodes in response to successive accretion onto the south Asian margin of the Qiangtang block in the Late Triassic, the Lhasa block in the Latest Jurassic–Early Cretaceous, and the Kohistan–Dras arc complex in the Late Cretaceous periods (Hendrix

et al., 1992; Dumitru *et al.*, 2001). The Late Jurassic event resulted in a widespread unconformity beneath the overlying Cretaceous strata that is recognized throughout much of the Tian Shan. During the Paleogene, the relative tectonic stability that prevailed in the Tian Shan (Bullen *et al.*, 2001, 2003; Sobel *et al.*, 2006) resulted in the beveling of topography and created several widespread regional unconformities (Burtman, 1975; Bullen *et al.*, 2001) that are documented in both the northern Chinese Tian Shan (Windley *et al.*, 1990; Allen *et al.*, 1993; Avouac *et al.*, 1993) and the Kyrgyz Tian Shan (Bullen *et al.*, 2001, 2003; Oskin & Burbank, 2005, 2007; Sobel *et al.*, 2006).

The Mesozoic strata deposited in the Tian Shan range are characterized by braided/meandering fluvial sediments and alluvial conglomerate (Hendrix *et al.*, 1992). Although these strata are dominated by subaerial deposits, Jurassic–Cretaceous organic or carbonate-rich strata provide evidence for local lacustrine environments at this time (Hendrix *et al.*, 1992; Deng *et al.*, 2000). Thick lower Tertiary fine-grained deposits (composed mainly of mudstone and siltstone) reveal that lacustrine environments existed intermittently in the northern Chinese Tian Shan foreland during the Early Tertiary. This interpretation is further reinforced by the presence of the gray, calcareous, Oligo-Miocene strata of the Huoerguosi anticline in the middle deformed zone (Fig. 1b, Deng *et al.*, 2000).

Our work is focused on the north flank of the Chinese Tian Shan, where thick Cenozoic deposits were shed into the Junggar foreland basin from the south. The present topography and high elevation of the Tian Shan are the result of north–south convergence driven by the India–Asia collision during Cenozoic times (Tapponnier & Molnar, 1979; Patriat & Achache, 1984; Avouac *et al.*, 1993) (Fig. 1a). Within the northern piedmont depression zone of the Tian Shan, this north–south compression produced three sub-parallel ridges of folds, known as fault-and-fold zones I–III, numbered sequentially outward from the mountains (Avouac *et al.*, 1993; Burchfiel *et al.*, 1999; Deng *et al.*, 2000; Fu *et al.*, 2003; Molnar *et al.*, 1994) (Fig. 1b). North-flowing rivers incise the anticlines perpendicular to strike where they expose thick successions of Cenozoic deposits. The Taxi He region (He is Mandarin for 'river') is a typical example, where the north-flowing Taxi He has sliced through the Tugulu anticline (Figs 1b and 2), thereby revealing well-exposed outcrops on the northern limb of this fold (Fig. 2).

The outcrop width of the Taxi He section approaches 2500 m (Figs 2 and 3a). In general, the dips of the exposed strata in the section gradually decrease northward from vertical beds near the core of the fold to $\sim 45^\circ$ at the top (Fig. 3a). A change of $> 10^\circ$ in dip occurs at ~ 350 m above the base of the section (Fig. 3a) and is interpreted as representing initial deposition of growth strata as discussed later. No significant faulting or major erosional discordance was found in the measured section, suggesting continuous deposition without significant breaks or duplication. The measured Taxi He section comprises three formations from base to top: the Taxihe, Dushanzi, and Xiyu Formations (Bureau of Geological and Mineral Resources of the Xinjiang Uygur Autonomous Region, 1993) with thicknesses of ~ 500, ~ 660, and ~ 40 m, respectively (Fig. 3a). Several hundred meters of poorly exposed Xiyu strata overlie the studied section. The Taxihe Formation consists dominantly of light brownish, fine-textured muddy siltstone and mudstone beds interbedded with coarse-grained sandstone or conglomerate deposits. The age of this formation in the northern Tian Shan foreland is inferred to be Miocene based mainly on the presence of Ostracoda fossils (Editing Committee of the Stratigraphy of China, 1999). The Dushanzi Formation primarily comprises coarse conglomerate, sandstone, and siltstone beds. According to the presence of the Ostracoda fossil group of *Ilyocypris–Cypideris–Candona* and mammalian fossil of *Hipparion*, the age of the Dushanzi Formation is traditionally inferred to be Pliocene (Editing Committee of the Stratigraphy of China, 1999). The Xiyu Formation, also known as the Xiyu conglomerate, is widespread in the piedmonts in northwest China (Liu *et al.*, 1996), where it typically consists of a thick sequence of gray or gray–black gravels in which some interbedded sands or sandy lenses are found, especially in the lowermost part. In most places, the dark Xiyu conglomerate clearly contrasts with the lighter colored Dushanzi conglomerates wherever they are juxtaposed. On the basis of the mammalian fossil *Equus sanmeniensis* found in a section located within the Anjihai anticline (Peng, 1975) to the west of Taxi He, the age of this formation is commonly inferred to be latest Pliocene to early Pleistocene.

MAGNETOSTRATIGRAPHY

Paleomagnetic sampling and methods

Paleomagnetic sampling was conducted along both the west and east bank of Taxi He (Figs 2 and 3a). Two or three samples were collected from each of 303 horizons, yielding a total of 676 samples for the Taxi He section. The vertical sampling interval varied between 0.75 and 13.4 m with an average interval of ~ 4 m. All the samples were collected with a portable drill and oriented with a magnetic compass that was corrected for the local magnetic declination anomaly (3.5°E in the Taxi He area). Most samples were collected from mudstone or siltstone beds. Where the deposits are predominantly conglomeratic, especially in the uppermost part of the sampled section, samples were collected in thin lenticular beds of siltstone or fine-grained sandstone. All the samples were cut into 2.0-cm long cylinders that were 2.5-cm in diameter.

Remnant magnetization was measured with a 2G cryogenic magnetometer at the Paleomagnetic Laboratory of the Institute of Geomechanics, Chinese Academy of Geological Sciences in Beijing. The magnetometer is located inside a set of large Helmholtz coils that reduced the ambient geomagnetic field to around 300 nT. One sample per horizon (a total of 303 pilot samples) was subjected to stepwise thermal demagnetization in an ASC

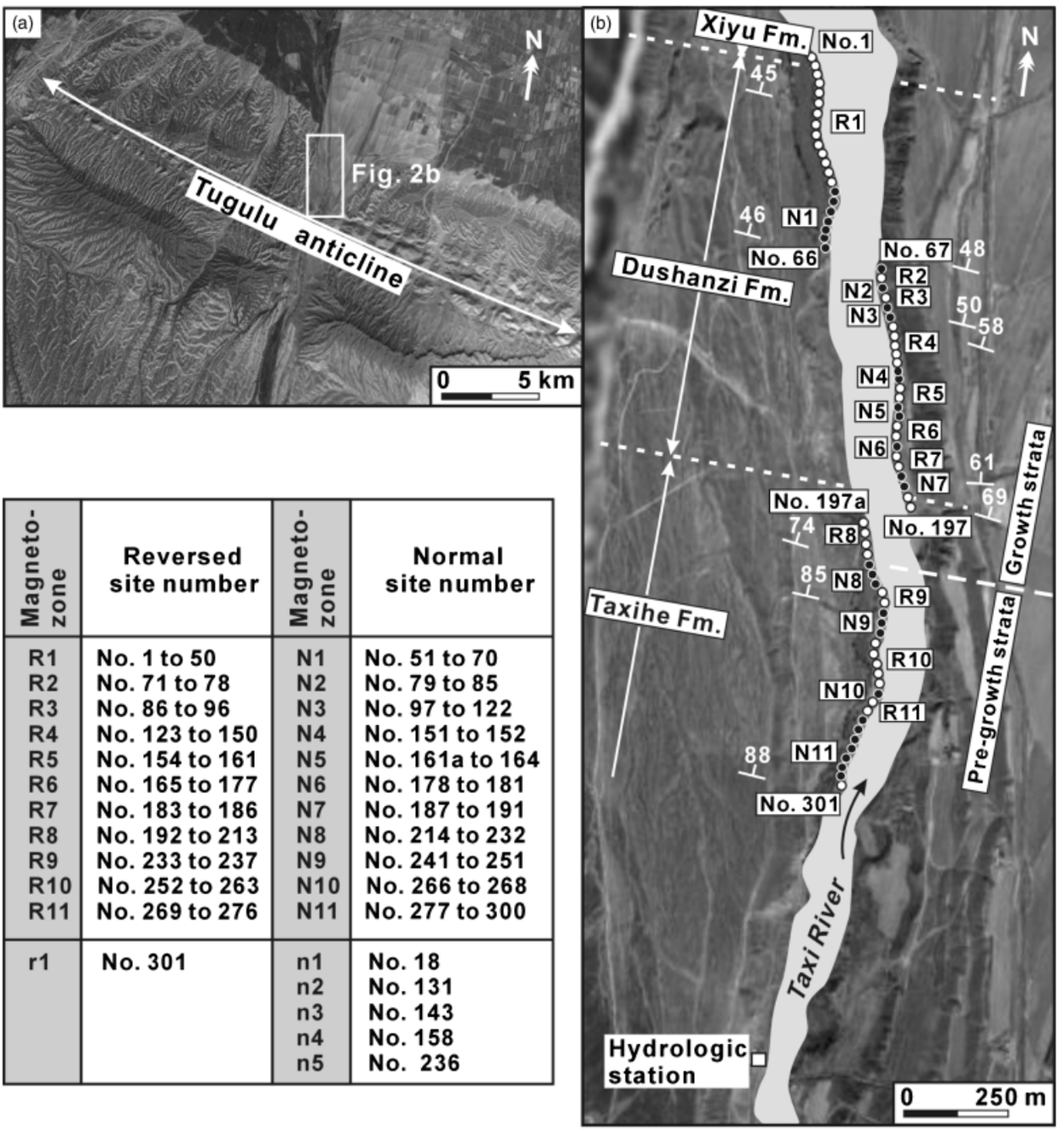

Magneto-zone	Reversed site number	Magneto-zone	Normal site number
R1	No. 1 to 50	N1	No. 51 to 70
R2	No. 71 to 78	N2	No. 79 to 85
R3	No. 86 to 96	N3	No. 97 to 122
R4	No. 123 to 150	N4	No. 151 to 152
R5	No. 154 to 161	N5	No. 161a to 164
R6	No. 165 to 177	N6	No. 178 to 181
R7	No. 183 to 186	N7	No. 187 to 191
R8	No. 192 to 213	N8	No. 214 to 232
R9	No. 233 to 237	N9	No. 241 to 251
R10	No. 252 to 263	N10	No. 266 to 268
R11	No. 269 to 276	N11	No. 277 to 300
r1	No. 301	n1	No. 18
		n2	No. 131
		n3	No. 143
		n4	No. 158
		n5	No. 236

Fig. 2. (a) Aerial photo view of the paleomagnetic sampling section in this study. (b) Locations of 303 magnetic sampling sites along Taxi River (all samples were collected in 2006). Normal (reversed) sites depicted as closed (open) circles. 'No. 1', 'R1', and 'N1' show the sampling site number and magnetozones of reversed or normal polarity, respectively. The site(s) contained in each magnetozone are listed in the lower left.

TD-48 oven with an internal residual field < 10 nT. For these samples, 13–17 steps were applied, commonly with the following stepwise heating routine: (i) 60°C steps up to 300°C; (ii) 40°C or 50°C steps up to 580°C; (iii) 30°C steps up to 640°C; and (iv) 20°C steps up to 680°C.

Demagnetization and statistical analysis

The intensities of the natural remanent magnetization (NRM) of the specimens were between 0.14×10^{-2} and 6.7×10^{-2} A/m with an average of $1.5 \pm 1.0 \times 10^{-2}$ A/m. Progressive demagnetization successfully isolated dominant magnetic components for the majority of the specimens after removing a viscous component of magnetization. According to their demagnetization behavior, all the samples are interpreted to display three major components (Fig. 4). A low-temperature component between 0°C and 180–240°C represents ~10–50% of the total remanence and is either normal polarity or overlaps with the next reversed component resulting in an undefined polarity direction. One or two intermediate temperature components (ITC), representing between 35 and 60%

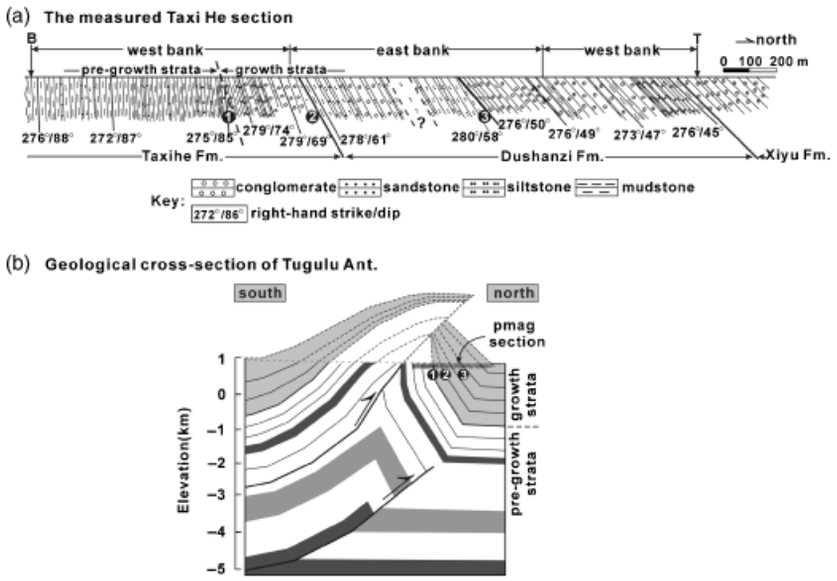

Fig. 3. (a) Measured geological section at Taxi He. Stratigraphic dips steepen southward from the lower part of the Lower Pleistocene Xiyu Formation (∼45°) to the upper Miocene Taxihe Formation (88°). 'T' and 'B' show the top and bottom of the Taxi He magneto-stratigraphic section, respectively. Solid numbered circles denote three abrupt changes in bedding dip. (b) Geologic cross-section of the Tugulu anticline along the Taxi He valley (modified from Burchfiel *et al.*, 1999). Based on the measured Taxi He section (a), the first change in dip is interpreted to represent the initial deposition of growth strata.

of the total remanence, are observed between 180–240°C and 540–580 °C. The ITC component is likely carried by magnetite or titanomagnetite, as suggested by the drop in remanence that occurs above 540–580 °C. Representing 10–40% of the total remanence, the high-temperature component (HTC) is manifested in a temperature range extending from ∼540–580°C to 610–680°C and commonly lies in the same direction as the ITC. This component is most likely carried by hematite or maghemite (Butler, 1992).

About 17 samples (out of 303 pilot samples) showed only unstable high-temperature demagnetization trajectories. For these stratigraphic horizons, another round of progressive thermal demagnetization was performed on a second sample. The characteristic directions of magnetization were determined by principal component analysis (Kirschvink, 1980). Data from a minimum of three, but more typically six to nine temperature steps, which were chosen above 450°C, were used for least-squares fits. About 10% of the samples displayed relatively scattered demagnetization directions. For these, the origin of the vector-component diagram was included as an additional datum when determining the characteristic directions of magnetization of these samples. For all samples, typical maximum angular deviation was between 1.2° and 15° with an average of 5.5 ± 2.9°. Based on the statistics of the best-fit lines, we eliminated 29 samples with poorly defined magnetic directions. The magnetic declination and inclination of the samples were then used to calculate virtual geomagnetic pole (VGP) latitudes. Samples with VGPs < 45° were not used for defining the magnetic polarity stratigraphy (MPS) for the Taxi He section except when they were adjacent to sites of the same polarity that showed VGPs > 45°. This filtering eliminated 28 sampled horizons. In total, 246 samples (one specimen per accepted horizon) were accepted to construct the MPS of the Taxi He section.

Reversal and fold tests were employed in order to discern the timing of characteristic remanent magnetization (ChRM) acquisition. Tilt correction significantly improves the grouping of ChRM poles (Fig. 5). The Fisherian site-averaged normal polarity and reversed polarity poles of the Taxi He section have an observed angular difference of 3.1° and a calculated critical angle of 9.8° [95% confidence level; assuming identical dispersion (K) values]. This indicates that the section passes the reversal test with a 'B' quality classification (McFadden & McElhinny, 1990). Because no samples were collected from the south limb of the Tugulu anticline, the simple fold test of McElhinny (1964) was used with K_{crit} defined as the statistical f distribution with $2(N-1)$ degrees of freedom, where N is the number of samples of a specified polarity. K_{crit} is compared with the ratio of K_2/K_1, where K_1 is the dispersion in geographic coordinates, and K_2 is the dispersion in tilt-corrected coordinates. A positive fold test for this section is indicated by the K_2/K_1 values of 1.53 (normal polarity) and 1.35 (reversed polarity), which are, respectively, larger than the K_{crit} values of 1.24 (normal) and 1.22 (reversed) at the 95% confidence level. Thus, the positive reversal and fold tests are interpreted to indicate that the ChRM directions were acquired by the sediments during or soon after deposition.

MPS

When constructing the MPS for the Taxi He section with VGP data, two samples with VGP latitudes < 45° were retained because they reinforce an adjacent, single, high-VGP-latitude site, and together these sites serve to define polarity zone N10 (Fig. 6d). Six magnetozones (n1–n5, r1) with only one sample are represented by a short half bar (Fig. 6d), and were not used to define the MPS of the Taxi He section or its correlation with the geomagnetic polarity time scale (GPTS). Overall, 11 normal (N1–N11) and 11 reversed (R1–R11) magnetozones are clearly identified in the

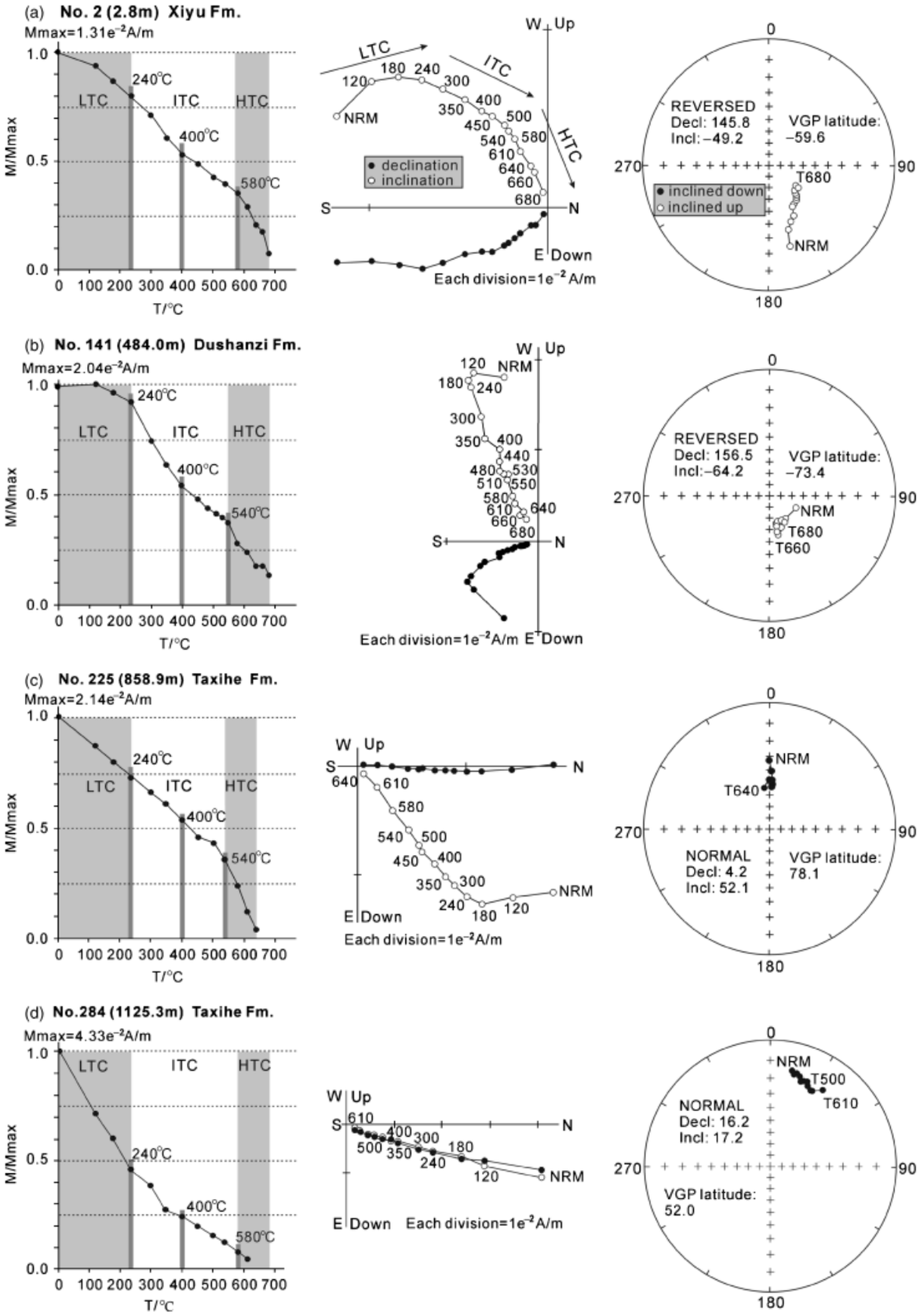

Fig. 4. Representative thermal demagnetization plots (remanent magnetic intensity graphs (left) and both Zijderveld diagrams (center) and equal-area projections (right) in tilt-corrected coordinates) typically showing three magnetic components. Examples of the low-temperature component (LTC), the intermediate temperature components (ITC), and the high-temperature component (HTC) of the characteristic remanence magnetization (ChRM) are depicted in (a). 300 = 300 °C.'No. 2 (2.8 m)' indicates the sample number with the corresponding stratigraphic level in the studied section.

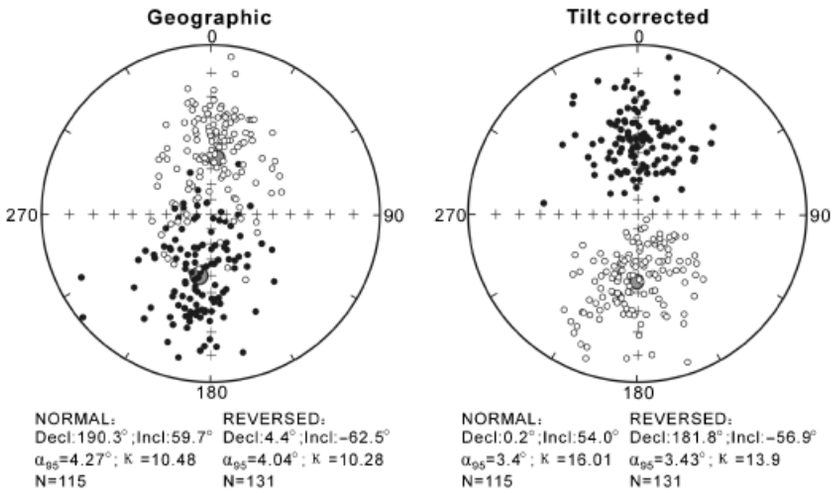

Fig. 5. Stereonet plots of palaeomagnetic data from the Taxi He section. Small solid (inclined down) and white (inclined up) circles indicate individual measurements with the larger circles showing the α_{95} error around the Fisher mean. Fisher's mean data are listed adjacent to each plot.

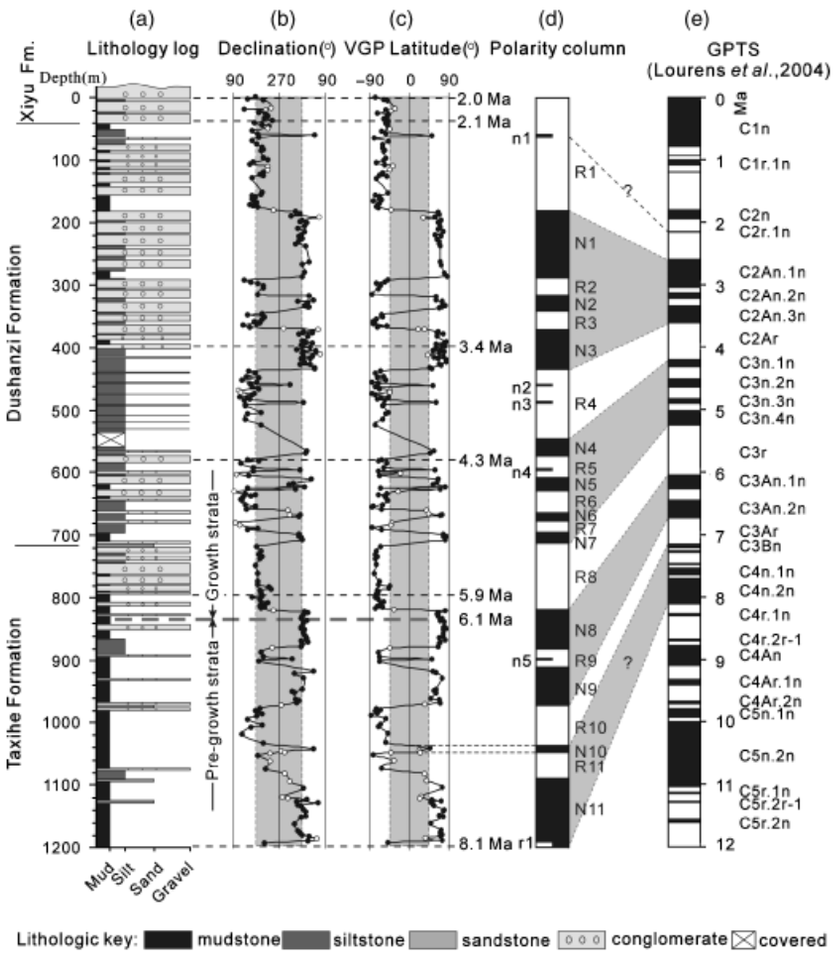

Fig. 6. Magnetic polarity stratigraphy (MPS) of the Taxi He section. (a) Lithology log with the base of growth-strata depicted at ~840 m depth (~6.1 Ma). (b) Magnetic declination in tilt-corrected coordinates (shaded zone equals 180°–360°). (c) Virtual geomagnetic pole (VGP) latitude. Open circles represent samples with absolute values of VGPs < 45°, which were not used to define the MPS of the Taxi He section except for the local magnetozone N10. Shaded zone equals ± 45°. (d) MPS defined commonly by samples with VGPs ≥ 45°. Black and white zones indicate normal and reversed polarity, respectively. Boundaries between magnetozones are defined by the midpoint between two samples with opposite polarity. Magnetozones defined only by one sample are displayed by short-half bars. Ages of stratigraphic and lithofacies boundaries are shown adjacent to the MPS. (e) Reference geomagnetic polarity time scale (GPTS) of Lourens *et al.* (2004).

Taxi He column (Fig. 6d). Each magnetozone is defined by at least three paleomagnetic samples from different sampled horizons. Our magnetostratigraphy was correlated with the GPTS of Lourens *et al.* (2004) (Fig. 6e) using the following characteristics: (1) three intervals with distinctive patterns of local magnetic polarity (N1–N3, N4–N7, and N8–N9), (2) four relatively long reversed magnetozones (R1, R4, R8, and R10), and one relatively long normal magnetozone (N11), (3) the absence of significant depositional interruption or faults throughout the section, (4) the presence of fauna/flora fossils (Peng, 1975; Editing Committee of the Stratigraphy of China, 1999) suggesting the probability that the Taxi He section has been sampled within Neogene to Lower Pleistocene strata, and (5) an assumption that sediment-accumulation rates vary systematically and relatively slowly.

Overall, our preferred correlation (Fig. 6d and e) successfully matches the major reversal patterns revealed in

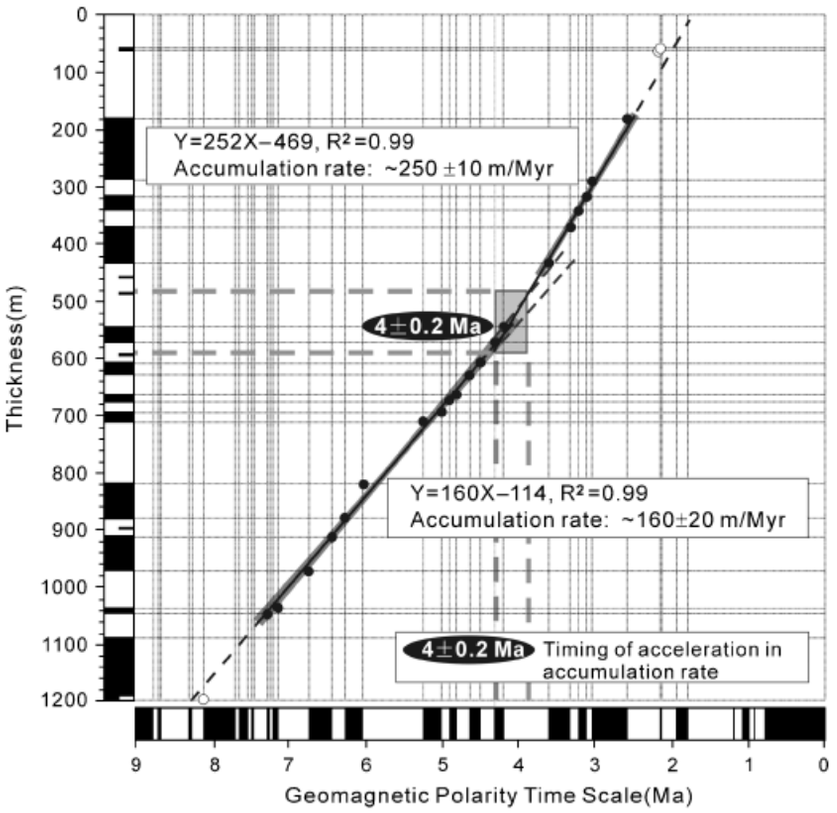

Fig. 7. Age versus thickness plot of the Taxi He section based on the correlation of Fig. 6d and e showing a $>50\%$ acceleration in sediment-accumulation rate at $\sim$4.0 Ma. The section has not been decompacted, and thus calculated sediment-accumulation rates represent minima. Shaded box depicts the range of likely ages for the acceleration in rates, based on a projection of the uncertainties on each regression (gray shaded envelopes).

the Late Miocene to Pliocene GPTS (Lourens *et al.*, 2004). Of course, some ambiguities remain with this correlation, for example, between normal magnetozones N10 and N11, where a few short-duration polarity events are missing in the Taxi He column. We matched N11 with the subchron C4n.2n based mainly on its relatively long span and on the correlation of the reversed magnetozone R10 with the subchron C3Ar. Despite inevitable uncertainties, the correlation, especially between N1-R10 and C2An.1n-C3Ar of the GPTS (Lourens *et al.*, 2004) (Fig. 6d and e), appears reasonable. The ages of the top and the base of the Taxi He section were calculated via a linear extrapolation of the sediment-accumulation rate in respective magnetozones N1 and R10, thereby constraining the sampled section to span from $\sim$8.1 to $\sim$2 Ma (Fig. 6). Similarly, the basal age of the Xiyu Formation is dated at $\sim$2.1 Ma. According to our preferred correlation, the relationship between the stratigraphic thickness and the magnetostratigraphic ages shows a significant increase in sediment-accumulation rate from $\sim$160 to $\sim$250 m Myr^{-1} at $\sim$4 Ma (Fig. 7), with an average rate of $\sim$200 m Myr^{-1} over the entire 6-Myr interval of the sampled section.

SEDIMENTOLOGIC ANALYSIS

Depositional evolution of the foreland since 8 Ma

Based on the magnetostratigraphic age controls, the first occurrence of thick conglomerate deposits in the Taxi He section occurs at $\sim$5.9 Ma (Fig. 6a). The two superposed parts of the Taxi He section separated by this age display distinct sedimentary characteristics. The strata deposited before $\sim$5.9 Ma comprise largely fine-grained mudstone and siltstone. In contrast, the strata accumulated after $\sim$5.9 Ma are dominated by coarse-grained conglomerates or pebbly sandstone. These two distinguishing lithofacies associations define the evolution of an alluvial–lacustrine depositional system in the Taxi He area.

Shallow lacustrine environment

The lowest part of the Taxi He stratigraphic section between $\sim$1200 and $\sim$800 m spans from $\sim$8.0 to $\sim$5.9 Ma and is dominated by thick (30–80 m), laminated or tabular, light brown mudstones and siltstones (Figs 6a and 8a). Relatively thin pebbly sandstone ($\sim$0.5–3-m thick) and conglomerate beds (up to 5 m thick) are intercalated within these thick fine-textured deposits, but represent $<10\%$ of the accumulated thickness (Fig. 8a). Erosional scours up to $\sim$1 m deep occur at the base of some of the thicker conglomerate beds. Sparse gypsum veins are also present within the lower part of the Taxi He section. Conglomerate interlayers are characterized by poorly sorted, subangular to subrounded clasts in a sandy matrix and by massive bedding or crude stratification.

The presence of horizontal bedding and gypsum, the well-preserved fine laminations, thick fine-textured deposits, and the absence of paleosols and mud cracks are interpreted as recording a shallow lacustrine environment in an arid setting (Ren & Wang, 1985; Magee *et al.*,

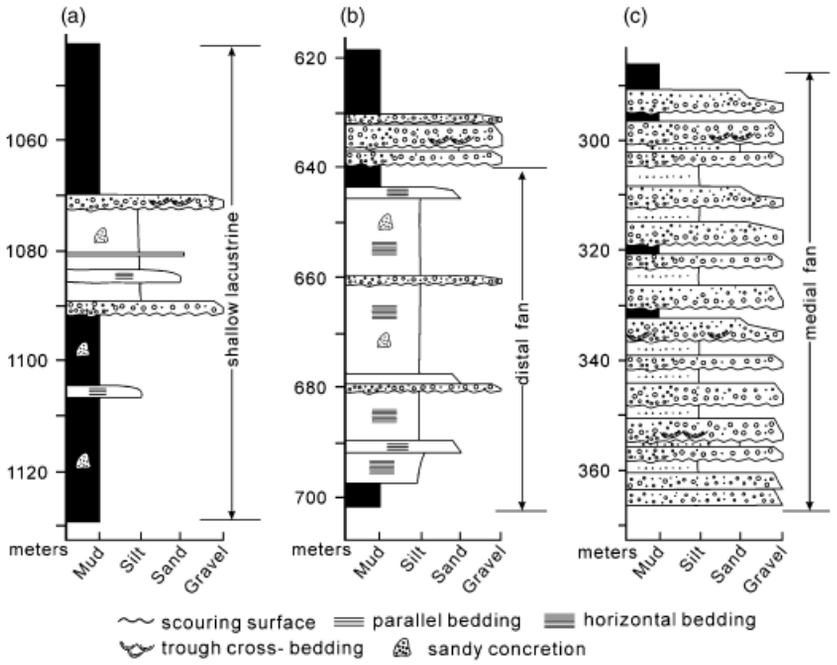

Fig. 8. Typical depositional rhythms in the Taxi He section. (a) Thick beds of fine-textured deposits intercalated with relatively thin beds of coarse-grained deposits in shallow lacustrine environment with distributary channels. (b) Alternation of thick siltstone and relatively thin sandstone and conglomerate interpreted as distal alluvial deposits. (c) Thick conglomerate beds interbedded with thin fine-grained beds in medial alluvial fan setting.

1995; Song *et al.*, 2001; Ortí *et al.*, 2003; Sun *et al.*, 2004, 2005a; Charreau *et al.*, 2005; Chen *et al.*, 2007; Heermance *et al.*, 2007). The lacustrine character of the fine-textured deposits that enclose the sand–matrix-supported, poorly sorted conglomerates suggests that these conglomeratic units could represent subaqueous gravity flows into a shallow lacustrine environment (Nemec & Steel, 1984; Ren & Wang, 1985).

Alluvial fan facies

In contrast to the fine-textured shallow lacustrine sediments, the deposits younger than 5.9 Ma are dominated by thick cobbly conglomerate beds interlayered with either thin beds of siltstone and muddy siltstone or lens/beds of sandstone. The overall coarse-grained deposition, however, is strikingly interrupted between ~400 and ~580 m (~3.4–4.3 Ma; Fig. 6) by continuous thick beds of siltstone and fine-grained sandstone.

The most common lithofacies assemblage typically consists of a composite unit of conglomerate, usually a few centimeters to several meters in thickness, commonly capped by siltstone or fine-grained sandstone and showing a crude fining-upward signature. The conglomerate deposits typically comprise clast supported, poorly sorted, subrounded to rounded clasts. Typically, the 10-m-thick conglomerate units are composed of several storeys that are each ~1–3 m thick. Individual beds commonly display massive bedding with subrounded, crudely imbricated clasts, and indistinct stratification. These coarse, amalgamated conglomerates are commonly capped by the 2- to 3-m-thick fine-grained sediments (Fig. 9b and c). Thinner conglomerate strata (few centimeters to decimeters in thickness) typify the stratigraphic section between ~400 and 580 m in the Taxi He section (Fig. 6a).

Evidence of scouring or channelized flow conditions, vague to less commonly distinct stratification of conglomerate deposits, and frequent alternation of thick beds of pebble or cobble conglomerates with relatively thin fine-grained deposits support the interpretation of an alluvial fan depositional environment since ~5.9 Ma in the Taxi He section for these terrigenous deposits (Miall, 1978; Nemec & Steel, 1984; DeCelles *et al.*, 1991; Blair & McPherson, 1994; Song *et al.*, 2001; Sun *et al.*, 2004, 2005a; Charreau *et al.*, 2005; Heermance *et al.*, 2007). These fan strata can be further divided into proximal, medial, and distal alluvium based on grain size, rounding, sedimentary structure, facies organization, and the nature of the contacts between different lithologic layers (Rust, 1978; Nemec & Steel, 1984; Ren & Wang, 1985). The proximal alluvial facies (Fig. 9a), equivalent to the deposits younger than ~2.1 Ma, is dominated by widespread cobble conglomerate and uncommonly contains interlayers or lenticular beds (usually a few centimeters to decimeters in thickness) of siltstone and fine-grained sandstone (Rust, 1978; Ren & Wang, 1985). This proximal alluvium is typified by the coarsest grain size, subangular clasts, and massive bedding, despite the uncommon presence of crude or distinct stratification. The medial alluvial facies (Fig. 9b) displays a typical depositional rhythm of high-energy braided channels consisting of thick beds of cobble conglomerate or coarse-grained sandstone interbedded with thin fine-grained beds (Fig. 8c). The metric-scale, fining upward trends are interpreted to result from waning discharge, typical of the deposits of many gravelly braided rivers (Miall, 1978; Nemec & Steel, 1984; DeCelles, 1994). The multi-storey conglomerates are interpreted to represent primary fan channels or moderately channelized flood events related to nearby channels (Nemec & Steel, 1984; DeCelles *et al.*, 1991; Song *et al.*, 2001; Heermance

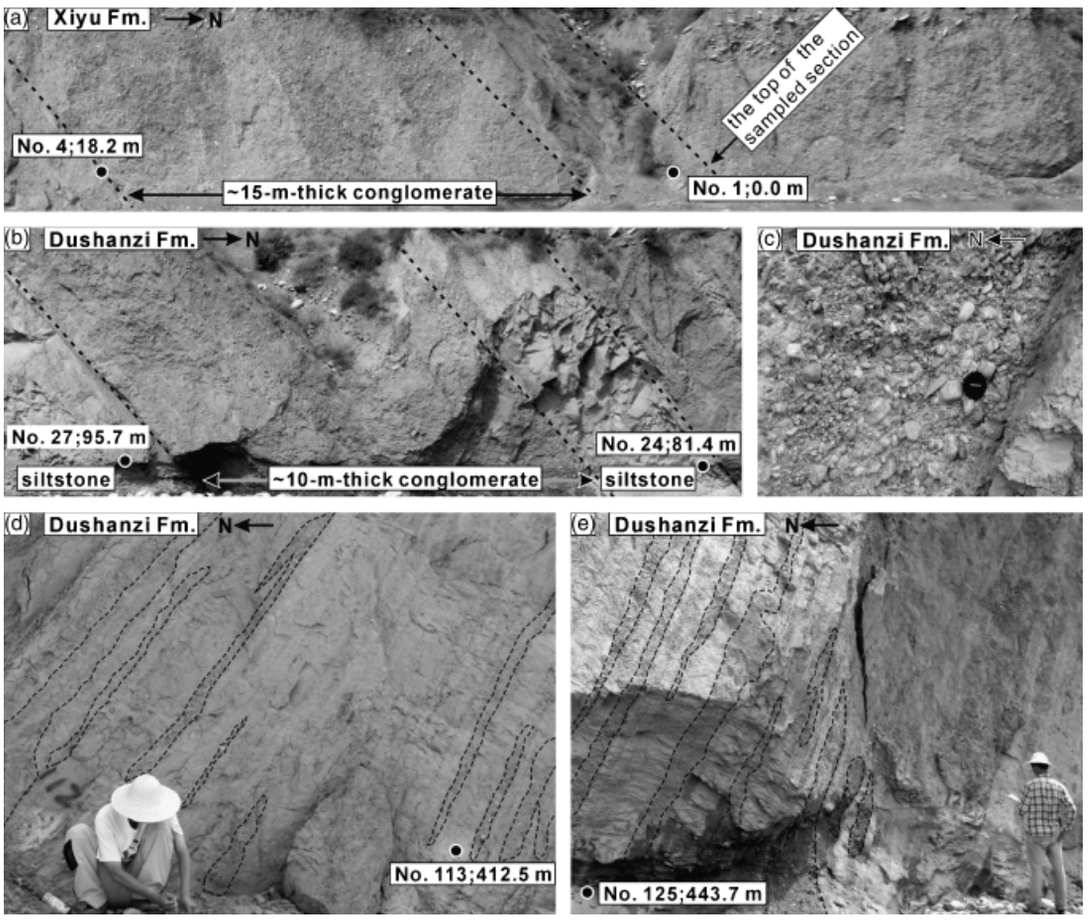

Fig. 9. Sedimentary characteristics in the Taxi He section with paleomagnetic sampling sites (solid circles) and stratigraphic level. (a) Continuous conglomerates lying stratigraphically above ~40 m depth in the section uncommonly contain interlayers or lens of fine-grained deposits. Black dashed lines denote the bedding of strata. Field view is ~30 m. (b) Strata in the upper Dushanzi Formation interpreted to represent a medial alluvial fan environment. 3-m-thick siltstone lies stratigraphically above ~10-m-thick conglomerate deposits. (c) Clast-supported, subangular-subrounded, crudely stratified and imbricated conglomerates in the medial alluvial fan environment at ~635 m depth. (d and e) Lower Dushanzi Formation interpreted as distal alluvial fan deposits, characterized by few-centimetre-to-decimeter-thick tabular and lenticular beds of coarse-grained deposits (usually sandy or pebbly conglomerate shown with dashed line) intercalated within thick siltstone deposits.

et al., 2007). The distal fan deposits (representing less-well channelized floodplain deposits) merge with the marginal lacustrine facies and dominantly comprise fine-textured sediments intercalated with thin beds (20–50 cm) of coarse-grained sandstone and pebbly conglomerate (Ren & Wang, 1985) (Figs 8b, 9d and e). Gypsum veins are present but uncommon in the distal fan facies.

Overall, the depositional evolution of the Taxi He section since 8 Ma can be divided into two distinct stages. Stage I ranges from ~8.0 to ~5.9 Ma, includes the middle and upper Taxihe Formation, and comprises predominantly fine-textured beds of mudstone and muddy siltstone that suggest a relatively low-energy environment interpreted as shallow lacustrine. Stage II ranges from ~5.9 to ~2.0 Ma and is equivalent to the uppermost Taxihe Formation, the Dushanzi Formation, and the lowest Xiyu Formation. These sedimentary facies are interpreted to be typical of a prograding and upward coarsening alluvial fan system, thus marking a significant shift from the previous lacustrine environment to a subsequent subaerial environment. Overall, this succession of stages results in an overall coarsening-upward sequence in the Taxi He area that implies a progradational depositional system in the northern Tian Shan foreland since at least late Miocene times.

Hierarchical sequence arrangement in the Taxi He section

The method of Lü *et al.* (2006) was used to probe the hierarchical sequence of Taxi He lithostratigraphy. First, lithologies of mudstone, siltstone, fine sandstone, medium sandstone, coarse sandstone, and conglomerate were assigned values of 5, 10, 20, 25, 30, and 45, respectively. Second, in order to give the same weight to each stratigraphic increment, every measured bed was represented as multiple 10-cm-thick beds of the same lithology as the

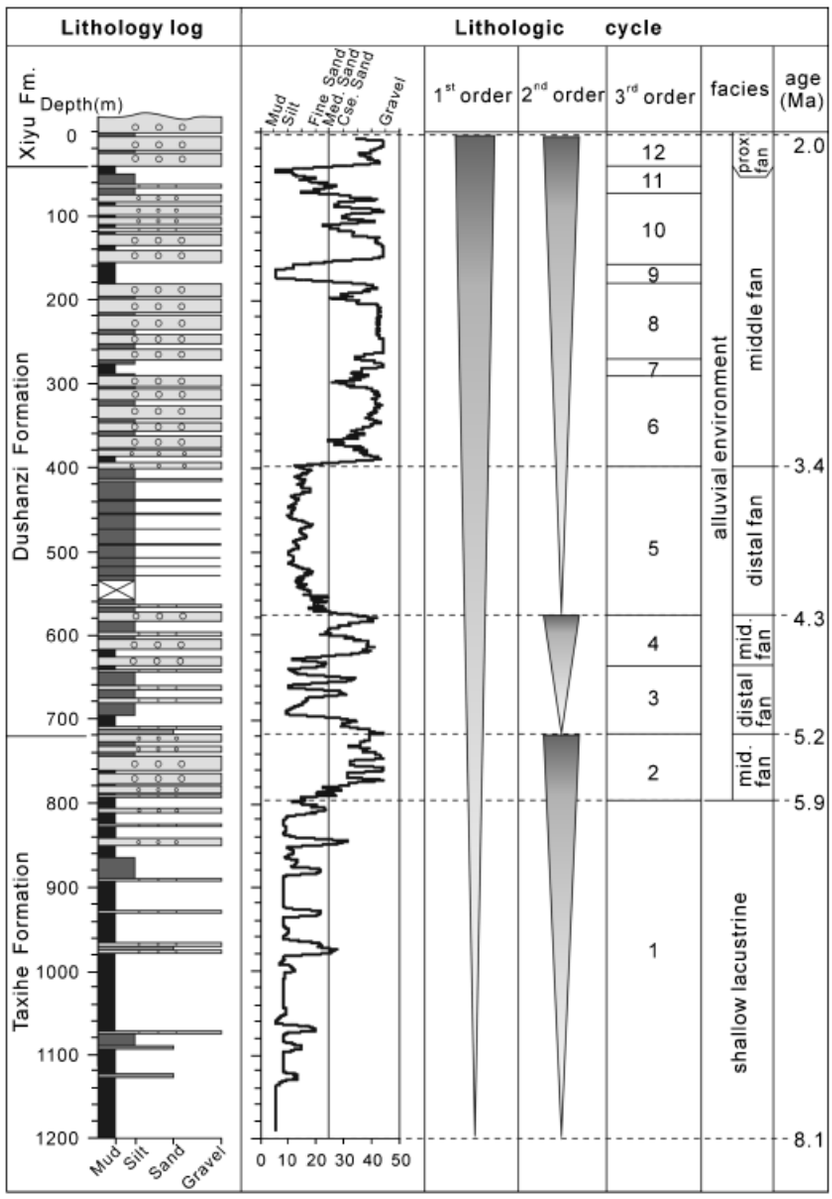

Fig. 10. Lithologic cycles of the Taxi He section. An arithmetic, 81-point moving average of grain size was used to define lithologic cycles. See text for the detailed description. Ages shown are based on magnestostratigraphic correlations in Fig. 6. See Fig. 6 for lithologic symbols.

original bed. When plotted against stratigraphic depth, an arithmetic, 81-point moving average of these 10-cm increments (equivalent to 8 m of sediment) clearly indicates the cyclic variations in lithology in the Taxi He section at several different temporal scales (Fig. 10).

A first-order upward coarsening trend is displayed by the vertical sequence of the whole depositional record in the Taxi He section (Fig. 10), corresponding to the vertical superposition of shallow lacustrine facies followed by alluvial deposits. Our magnetostratigraphic study assigns the first-order sequence a minimum span of ~6 Myr (Fig. 10). Similar to some previous studies (e.g. Burbank *et al.*, 1988; DeCelles & Giles, 1996; DeCelles *et al.*, 1998; Chen *et al.*, 2002, 2007; Heermance *et al.*, 2007), we interpret this large-scale coarsening-upward sequence at Taxi He to represent a progradational depositional system controlled by progressive tectonic deformation that encroached on a foreland and drove lateral facies migration. In contrast, Sun *et al.* (2004) interpreted the first occurrence of thick conglomerates as the direct indicator of initial, coeval tectonic uplift of Tian Shan. Such an interpretation seems unlikely to be correct, however, because conglomeratic facies progradation is time transgressive (e.g. Burbank *et al.*, 1988; DeCelles & Giles, 1996; Chen *et al.*, 2002, 2007; Charreau *et al.*, 2005; Heermance *et al.*, 2007), and time lags exist among different types of sedimentary indicators of tectonism in alluvial foreland basin settings (Burbank *et al.*, 1988; Jordan *et al.*, 1988; Jones *et al.*, 2004; Heermance *et al.*, 2007).

Encompassed within this overall trend, three second-order coarsening-upward sequences are interpreted to represent meso-scale progradational processes (Fig. 10). Each second-order sequence spans a period of ~1–3 Myr based on the magnetostratigraphy and ranges from ~160 to 560 m in thickness (Fig. 10). Third-order intervals are mainly represented by the alternation of fine-grained

assemblages (usually mudstone and siltstone) and coarse-grained conglomerate packets. We identify 12 third-order intervals in the Taxi He succession (Fig. 10), each of which has a duration of ~100–500 kyr. Generally, each conglomerate packet is thicker than the associated fine-grained assemblage, excepting third-order sequences 1, 3, and 5 (Fig. 10). The third-order cycles 3 and 5 are interpreted as representing distal fan (floodplain) deposits (Fig. 10).

Beyond the above hierarchical sequence arrangement, smaller-scale lithologic variation is recorded by alternation of thick conglomerates with thin beds of fine-grained sandstone or siltstone within coarse conglomerate packets (Fig. 10). This pattern is interpreted as the result of the abandonment and migration of braided channels (Nemec & Steel, 1984; DeCelles *et al.*, 1991; Song *et al.*, 2001; Heermance *et al.*, 2007).

As described by Charreau *et al.* (2005) and Sun *et al.* (2004), the Dushanzi section (see Fig. 5 of Sun *et al.*, 2004) and the Kuitun He (east) section (see Fig. 2 of Charreau *et al.*, 2005) also show a large-scale coarsening upward sequence during Late Cenozoic times that is similar to that of the Taxi He section. Although separated by up to ~130 km along strike in the Junggar foreland, all these sections record similar stages of depositional evolution: a progradational depositional succession that evolves from older lacustrine facies to a younger alluvial environment (Sun *et al.*, 2004; Charreau *et al.*, 2005; this study). Thus, the establishment of the first-order upward coarsening sequence and its correlation in the northern Chinese Tian Shan foreland can be easily recognized. In contrast, because of the transverse variation in depositional systems along the north piedmont of the Tian Shan that results from both the spacing of individual river systems and the activity on numerous discrete structures within the foreland, second- and third-order sequences are unlikely to correlate across the entire foreland.

DISCUSSION

Correlations among north Tian Shan magnetostratigraphic sections

Over the past several years, Charreau *et al.* (2005) and Sun *et al.* (2004, 2007) published new magnetostratigraphies from three closely spaced sections near Dushanzi (Fig. 1b): one is located on the eastern end of the Dushanzi anticline (Sun *et al.*, 2004), the other two lie ~5 km farther west along the east and west bank of Kuitun He where it flows across this fold. These three sections lie ~130 km west of the Taxi He section (Fig. 1b). We refer to them as the Kuitun He (west) section (Sun *et al.*, 2007), the Kuitun He (east) section (Charreau *et al.*, 2005), and the Dushanzi section (Sun *et al.*, 2004), respectively (Fig. 11). Because they each span overlapping parts of the upper Cenozoic succession, we have correlated their reversal patterns with each other and to the Taxi He section based on lithostratigraphy and reversal patterns (Fig. 11). Here, we support the re-correlations of the Dushanzi section (Sun *et al.*, 2004) and the Kuitun He (west) section (Sun *et al.*, 2007) as proposed by Charreau *et al.* (2005, Fig. 6; 2008a, Fig. 2) for the following reasons. According to the lithologic logs (Fig. 2, Charreau *et al.*, 2005; Fig. 5, Sun *et al.*, 2004; Fig. 8, Sun *et al.*, 2007) and the description on paleomagnetic sampling, we infer that they both identify the base of the Xiyu conglomerate at about the same stratigraphic level within the Dushanzi anticline with respect to the onset of very continuous conglomeratic facies. Accordingly, the basal ages of the Xiyu conglomerate in these three nearby sections should approximate each other. As originally published, however, these ages differed by >2 Myr: 2.6 Ma in the Dushanzi and Kuitun He (west) sections vs. 4.8 Ma in the Kuitun He (east) section. We argue that the Xiyu conglomerate is unlikely to be so starkly diachronous across a short distance parallel to strike. We consider Charreau *et al.*'s (2005) overall correlation to be more convincing due to the longer time spanned by their section and the need for fewer abrupt, large changes in accumulation rates in comparison with Sun *et al.*'s (2004, 2007) correlations. Not surprisingly perhaps, this recorrelation yields a more consistent basal age for the Xiyu conglomerate in these nearby sections. Because correlations to the Gilbert chron (C2Ar-C3r: Fig. 11) are somewhat ambiguous in these magnetostratigraphies, the Xiyu conglomerate's basal age still retains some uncertainty. Despite this, the onset of Xiyu deposition (Fig. 11) is likely to be ~0.5 Myr younger at Dushanzi (~4.2 ± 0.2 Ma) than in the Kuitun He sections (~4.7 ± 0.2 Ma) that are ~5 km away.

Timing, magnitude, and patterns of foreland deformation

North of the Junggar Frontal Thrust, three elongate zones of sub-parallel folds (Fig. 1b) record the progressive encroachment of deformation into the foreland during the Neogene. Growth strata, limb rotation, and angular unconformities in the anticlines of the three east–west trending fault-and-fold zones (Fig. 12) provide evidence for prolonged, but episodic deformation within the Tian Shan. The Qigu anticline is located in fault-and-fold zone I (Fig. 1b) and comprises Jurassic, Cretaceous, and Tertiary strata (Fig. 12c). The unconformable contact between the upper Jurassic and the lower Cretaceous strata indicates significant deformation across the region during Late Mesozoic times (Hendrix *et al.*, 1992; Burchfiel *et al.*, 1999; Deng *et al.*, 2000). The generally parallel dips and conformable contacts of the Cretaceous through Neogene strata on the northern limb of this fold (Fig. 12c), however, suggest that, for more than 100 Myr before the late Tertiary, no significant deformation disrupted deposition (Bullen *et al.*, 2001, 2003; Sobel *et al.*, 2006). Folding of Neogene strata in Qigu's northern limb indicates renewed deformation sometime in the last 20 Myr, but no precise limits can be placed on its initiation in this fold. Further west in zone I, on the northern limb of the Tuostai anticline, geometric constraints and seismic interpretations require abrupt thinning of Pliocene strata onto the fold (Fig. 12a), thereby

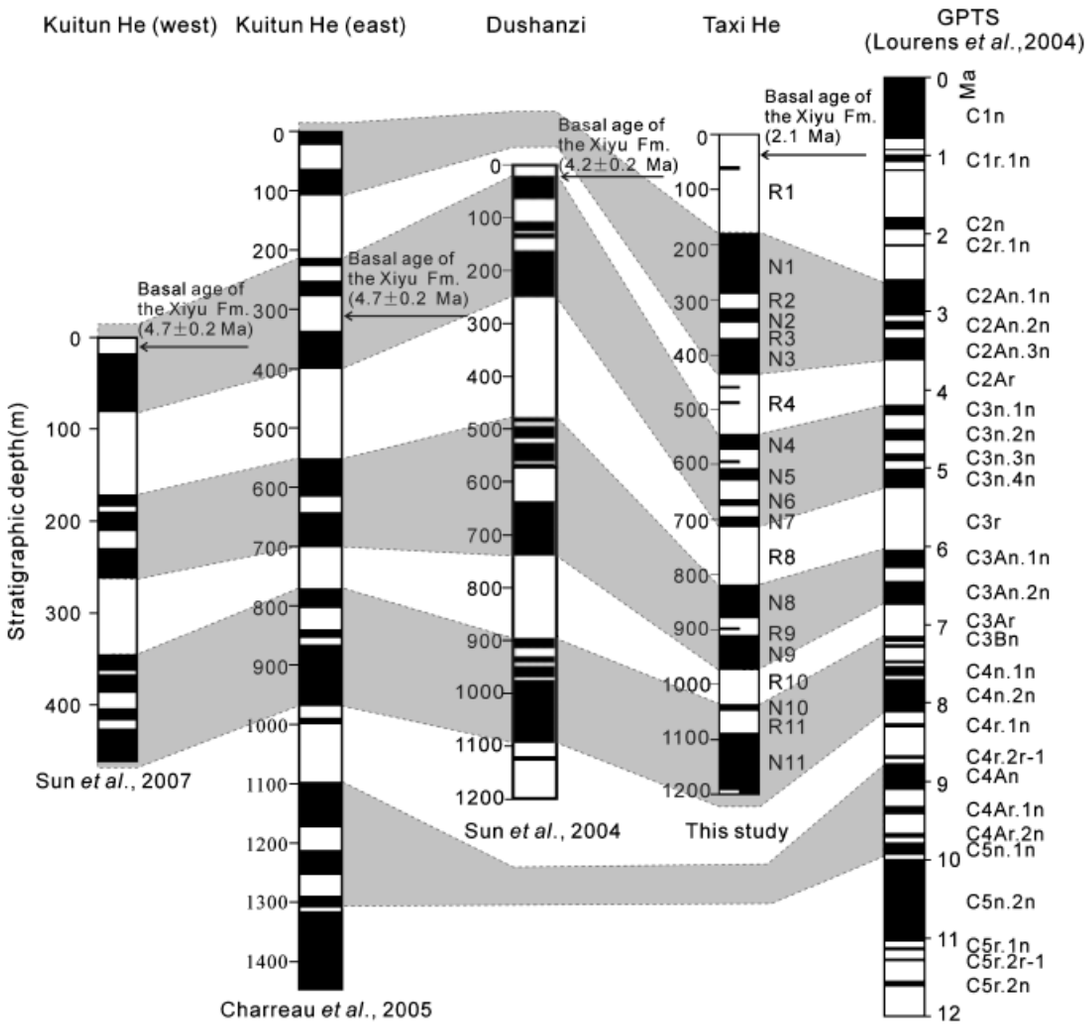

Fig. 11. Correlations among MPSs of the Kuitun He (west) section (Sun *et al*., 2007), the Kuitun He (east) section (Charreau *et al*., 2005), the Dushanzi section (Sun *et al*., 2004) and the Taxi He section (this study). The basal ages of the Xiyu conglomerate in these four sections also are shown adjacent to the corresponding magnetic columns.

implying Pliocene fold growth. Here, it appears that folding continued through deposition of the Xiyu conglomerate, which is also deformed on the northern limb of the fold. Undeformed Late Quaternary terraces of Hutubi River cutting the Qigu anticline (Deng *et al*., 2000) imply that this anticline is currently inactive.

The best-dated structure in the medial deformed foreland zone (fault-and-fold zone II) is the Tugulu anticline. The topographic expression of this fold strikes approximately east–west, and is ~50 km long and ~8 km wide (Fig. 2a). As a north-vergent fault-propagation fold (Burchfiel *et al*., 1999), the asymmetric Tugulu anticline displays steeper strata on its forelimb (Fig. 3), where the measured Taxi He section reveals a systematic decrease in dip from nearly vertical beds near the core of the fold to ~45° at the top of the section (Fig. 3a). A unconformity occurs at ~350 m above the base of the section (labeled with the number '1', Fig. 3a) where depositional onlap across a 10° discordance in dip is interpreted as representing the initial deposition of growth strata (Fig. 3b) when folding of the Tugulu anticline commenced. Over the next ~150 m of strata, the dip progressively decreases by another 13°: an observation consistent with growth strata, rather than with simple dip panels (Suppe *et al*., 1992). In contrast, some other dip changes, for example, at 790 m height (labeled '3' in Fig. 3a), discretely separate zones of quite uniform dips, suggesting folding across axial surfaces. Based on the position of the growth strata within our magnetostratigraphy, folding of the Tugulu anticline commenced at ~6.1 Ma (Figs 3 and 6). The youngest strata in our section date from ~2 Ma and dip at 45°, indicating that over half of the limb rotation has occurred since 2 Ma. Late Pleistocene terraces are deformed across the Tugulu anticline (Burchfiel *et al*., 1999). Hence, the growth of the Tugulu fold has spanned ~6 Myr. In the absence of seismic data to illuminate stratal geometries in the subsurface, we note that our interpretation of growth strata is based on the bedding–dip relationships and depositional onlap described above. The lack of subsurface data for this fold precludes a truly unambiguous interpretation.

The Dushanzi anticline in fault-and-fold zone III exposes folded Neogene–Pleistocene strata (Fig. 12b). Here,

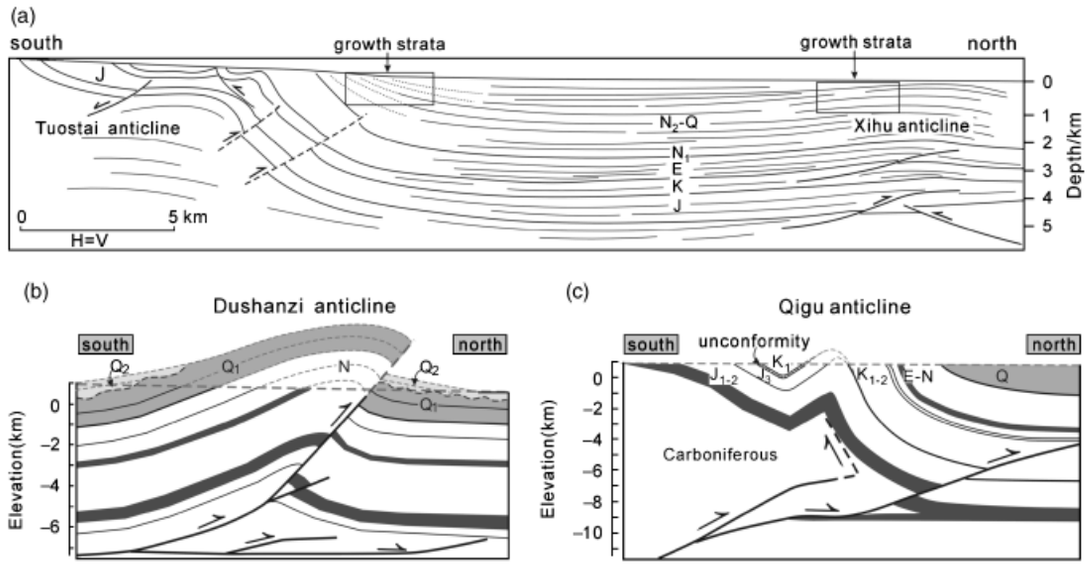

Fig. 12. Structural cross sections depicting deformation and cross-cutting relationships in the northern Tian Shan foreland. For section locations, see Fig. 1b. (a) Line drawing of seismic profile through the Tuostai and Xihu anticlines (modified from Xu *et al*., 1992). Growth strata are identified in the Pliocene-Quaternary deposits of Xihu and Tuostai anticlines. J, K, E, N_1, N_2, Q are the Jurassic, Cretaceous, Paleogene, Miocene, Pliocene and Pleistocene, respectively. (b) Geological section of the Dushanzi anticline along the Kuitun He valley (modified from Burchfiel *et al*., 1999). Middle Pleistocene strata (Q_2) unconformably overlie lower Pleistocene strata (Q_1) (Deng *et al*., 2000), indicating Early Pleistocene deformation of the Dushanzi anticline. (c) Geological section of the Qigu anticline along the Hutubi He (modified from Burchfiel *et al*., 1999). An anticline–syncline pair lies north of a gently N-dipping section of Jurassic strata. Unconformity between the upper Jurassic (J_3) and lower Cretaceous (K_1) strata implies Mesozoic deformation at Qigu (Burchfiel *et al*., 1999; Deng *et al*., 2000). Uniform steep north dips ($>60°$) and comformable contacts of Cretaceous (K) through Neogene (E) strata, however, suggest tectonic quiescence until the late Tertiary. Folding postdates deposition of Neogene strata preserved in the northern limb of the anticline.

a middle Pleistocene unconformably truncates the lower Pleistocene Xiyu conglomeratic (Fig. 12b; Deng *et al*., 2000), indicating significant folding of the Dushanzi anticline sometime in Early to Middle Pleistocene times (Deng *et al*., 2000; Fu *et al*., 2003). As at Tugulu, deformed flights of terraces indicate that folding has continued until present (Molnar *et al*., 1994). To the north of the traditionally delineated fault-and-fold zone III, Pleistocene growth strata that are revealed by seismic lines (Xu *et al*., 1992) help define the presently active Xihu anticline (Fig. 12a): the outermost fold currently developing in the north piedmont of Chinese Tian Shan (Fig. 1b). Because foreland subsidence and sediment-accumulation rates have outpaced the rate of vertical anticlinal growth, the Xihu anticline has little to no surface expression (only 10 m topographic relief). Nonetheless, ~500 m of structural relief has developed in the subsurface according to the seismic section (Fig. 12a; Xu *et al*., 1992).

The post-Triassic detrital strata in the Junggar foreland basin taper progressively northward from a thickness of 6–9 km near the Junggar frontal thrust to 4–5 km at the northern limit of deformation (Fig. 13). At the base of the Jurassic, a detachment horizon is interpreted to have accommodated most of the fault-localized slip as deformation stepped out into the foreland (Fig. 13). In zone I, a large fault-bend fold (Figs 12 and 13) accounts for most of the shortening in the innermost fold, although several thrusts cause localized folding above the basal detachment. Farther north, thrust faults are interpreted to ramp from the basal Jurassic detachment toward the surface where they modulate the deformation of the well-studied suite of fault-propagation and fault-tip folds in zones II and III (Deng *et al*., 1991, 2000; Avouac *et al*., 1993; Burchfiel *et al*., 1999; Daëron *et al*., 2007).

Shortening estimates (Table 1) have previously been calculated for most of the anticlines in the northern Tian Shan foreland. For the Nanmanasi anticline (which we did not map) in the east part of zone I, we tentatively estimate a shortening of ~4–6 km (Table 1), on the basis of the shortening magnitude of other anticlines in fault-and-fold zone I. If this estimate is acceptable, then when combined with previous shortening estimates (Deng *et al*., 1991, 2000; Molnar *et al*., 1994; Yang *et al*., 1996; Burchfiel *et al*., 1999; Daëron *et al*., 2007; Charreau *et al*., 2008b), these data (Table 1) permit us to examine the regional patterns of shortening along and across strike in the foreland (Fig. 14). Overall, the total magnitude of Neogene shortening across the foreland ranges from ~8 to ~15 km, but within each fault-and-fold zone, the magnitude of shortening varies along strike. In fault-and-fold zone II, for example, adjacent anticlines show ~6–10 km of shortening in the eastern two-thirds of the study area, whereas the magnitude of shortening markedly diminishes to the west (Figs 12a and 14). In zone III, active fold growth in the west accommodates ~1–3 km of shortening, whereas no folding is recorded in this zone farther to the east (Figs 1b and

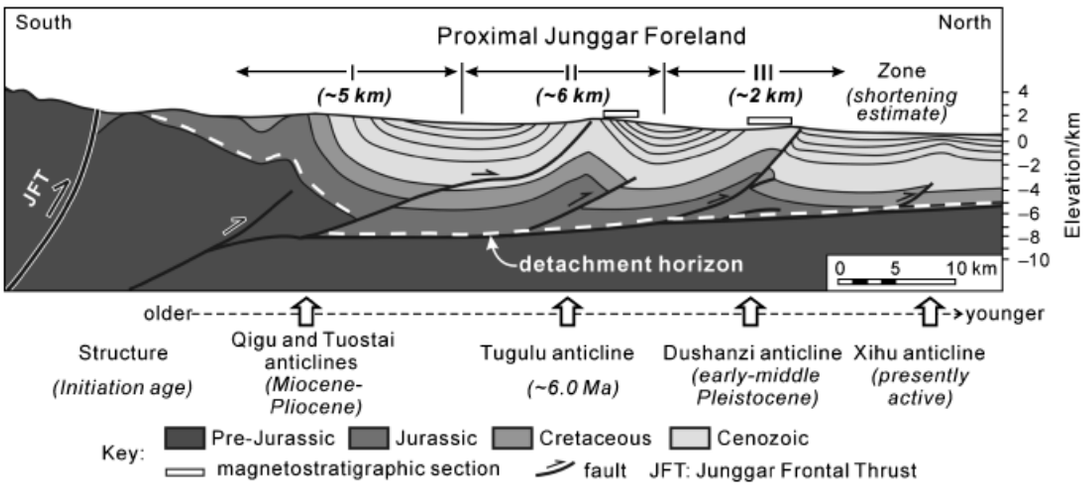

Fig. 13. Generalized geological cross-section of the northern Chinese Tian Shan foreland showing major thrust faults, detachments, and fault-and-fold zones. The total stratigraphic thickness of Mesozoic and Cenozoic strata is ~7–12 km (Cenozoic: ~3–5 km thick), and fault ramps underlying the anticlines in each deformed zone dip ~20–60° (Xu *et al.*, 1992; Burchfiel *et al.*, 1999; Deng *et al.*, 2000). A major detachment horizon is interpreted as a lower Jurassic composite of shale, mudstone, and coal measures that attains ~600 m in thickness, is located at between ~7 and 9 km depth (Deng *et al.*, 2000), and converges southward with the Junggar Frontal Thrust. Shortening is estimated for anticlines in each fault-and-fold zone (Table 1). Interpreted ages for initiation of folding within each zone suggest progressive migration of tectonic deformation northward into the foreland.

Table 1. Minimum shortening estimates of anticlines across the fault-and-fold zones of the northern Tian Shan foreland

Fault-and-fold zone	Shortening estimates (km)	References
I		
Tuostai anticline	~4.6–5.0	Burchfiel *et al.* (1999)
Nananjihai anticline	> 4.2	Deng *et al.* (2000)
Nanmanasi anticline	~5	This study
Qigu anticline	6.2	Burchfiel *et al.* (1999)
	5.5	Deng *et al.* (2000)
II		
Huoerguosi anticline	~10	Charreau *et al.* (2008b)
Manasi anticline	~6.5	Deng *et al.* (2000)
Tugulu anticline	6.0	Yang *et al.* (1996)
	5.5	Burchfiel *et al.* (1999)
		Molnar *et al.* (1994)
III		
Dushanzi anticline	2.12–2.35	Burchfiel *et al.* (1999)
		Molnar *et al.* (1994)
	2.9	Deng *et al.* (2000)
Anjihai anticline	1.5	Daëron *et al.* (2007)
		Deng *et al.* (1991)

14). The locus of maximum shortening switches between zones I and II along strike, but never occurs in zone III, where the duration and intensity of folding are the least. The general consistency of total shortening across the foreland suggests that tectonic forcing was spatially uniform during Late Cenozoic times along this ~130-km-long swath of the northern Tian Shan foreland. Whether that shortening was absorbed primarily in the most proximal foreland structures (zone I) or in more distal folds (zone II in the east) probably depended on how shortening was fed into the detachment along strike and whether pre-existing structures in the Triassic and older bedrock were reactivated during the Neogene.

Despite shortening estimates for numerous individual anticlines (Table 1), calculation of long-term shortening rates for all these folds is difficult, because the time of initiation of deformation is poorly known. Based on assumptions that the Xiyu conglomerate could be treated as a chronostratigraphic unit with a basal age of ~2.5 Ma throughout the Tian Shan and that deformation began some time after initial Xiyu deposition, Burchfiel *et al.* (1999) calculated the shortening rates for several folds in both the north and south flanks of the Tian Shan. These simplifying assumptions, however, are violated both by the strongly diachronous base of the Xiyu conglomerate in this region (Fig. 11) and by more recent interpretations placing the start of deformation significantly before the onset of conglomeratic deposition for some folds. For the Tugulu anticline, for example, we calculate a shortening rate using a ~6.0-Ma age for the initiation of folding based on our dated growth strata (Fig. 6). When combined with a total shortening of ~5.5–6.0 km estimated by Burchfiel *et al.* (1999) and Yang *et al.* (1996), this age yields an average rate of ~0.9–1.0 mm yr^{-1}. Within the dated section at Dushanzi anticline (Charreau *et al.*, 2005), the steadiness of sediment accumulation and the absence of recognized growth strata suggest that folding there began after 3 Ma, thereby providing a lower limit on the shortening rate of $\geq$ 0.7 mm yr^{-1}. Using a fault-tip fold growth model of the Anjihai anticline and magnetostratigraphic ages (Charreau *et al.*, 2005) extrapolated from the Dushanzi fold (~45 km to the west), Daëron *et al.* (2007) estimated that, deformation began at Anjihai at ~7 Ma. Based on

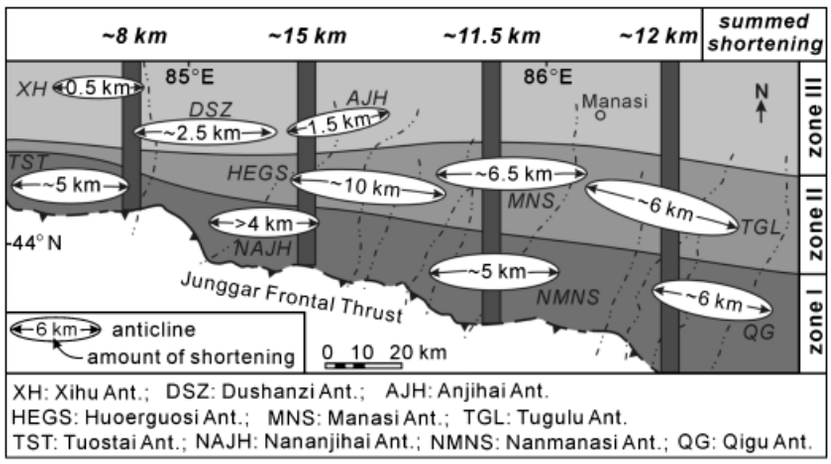

Fig. 14. Shortening estimates of anticlines in the northern Tian Shan foreland. Total magnitude of shortening across the foreland ranges from ~8 to 15 km, whereas the magnitude of shortening varies within each fault-and-fold zone along strike. The data are from Table 1.

observed geomorphic and structural constraints at the surface, they further argue that, despite a mean long-term shortening rate of $\sim 0.2\,\mathrm{mm\,yr^{-1}}$, rates have recently accelerated to $\sim 1\,\mathrm{mm\,yr^{-1}}$ and were only $\sim 0.1\,\mathrm{mm\,yr^{-1}}$ for most of the Anjihai's shortening history. The apparent depth of growth strata in the Xihu seismic data (Fig. 12a), its seismic similarity to the Anjihai (Daëron *et al.*, 2007), the absence of a significant topographic expression of the Xihu fold, and its distal position with respect to the Dushanzi fold where Mio-Pliocene sedimentation rates were $\sim 0.2\,\mathrm{mm\,yr^{-1}}$ argue for sustained slow growth of the Xihu fold, analogous to that at Anjihai anticline.

Whereas we now have substantial insight on shortening rates within fault-and-fold zones II and III in the northern Tian Shan foreland, zone I is only broadly dated. Better understanding of the shortening history across the foreland requires significantly improved chronological constraints on deformation of these undated folds.

Structural controls on depositional evolution and accumulation rates

Sedimentation patterns in foreland basins are sensitive to the distance to the front of the orogenic wedge, to the character of the rocks that are being raised above base level within the foreland due to ongoing deformation, and to reorganization of sediment distribution systems by growing folds and active faults (e.g. Colombo, 1994; Burbank *et al.*, 1996; DeCelles & Giles, 1996; Tucker & Slingerland, 1996; DeCelles *et al.*, 1998; Chen *et al.*, 2002, 2007; Parès *et al.*, 2003; Charreau *et al.*, 2005; Heermance *et al.*, 2007). Typically, proximal coarse-grained deposits are deposited coevally with distal, finer-grained deposits within a subsiding foreland (Heller *et al.*, 1988; Charreau *et al.*, 2005; Heermance *et al.*, 2007). The progressive encroachment of deformation into the foreland drives a tendency for deposition at any given site to coarsen upwards through time, as the entire alluvial system progrades outward into the foreland basin. During this process, older, more proximal strata become gradually deformed both at and behind the leading edge of encroaching structural disruption, whereas growing folds commonly deflect fluvial channels and cause lateral shifts in the loci of deposition (Heller & Paola, 1992; Burbank *et al.*, 1996, 1999; DeCelles & Giles, 1996). Structural encroachment into a foreland is also expected to drive an overall acceleration in the rate of sediment accumulation as the locus of tectonic loading approaches any given site. As seen in many forelands, however, tectonic encroachment is not a steady, incremental process, but rather consists of episodic forward steps as older, more proximal faults and folds are abandoned and new, more distal ones are formed. This step-wise encroachment should generate coeval accelerations in sediment-accumulation rates in front of newly developing tectonic loads.

In the Taxi He area, a first-order upward coarsening cycle is defined by the lacustrine depositional environment that dominates until ~6 Ma and is succeeded by strata deposited by braided rivers and alluvial fans (Fig. 10). Upward coarsening also characterizes the foreland sections in the Dushanzi area (Sun *et al.*, 2004; Charreau *et al.*, 2005) and is consistent with the expectation of a clastic wedge prograding from the deformed hinterland. More detailed insight on tectonic controls emerges from analysis of the sediment-accumulation rate curve from the Taxi He section (Fig. 7). The magnitude of the acceleration in sediment-accumulation rate at 4 Ma is striking: a $>50\%$ increase from ~160 to $\sim 250\,\mathrm{m\,Myr^{-1}}$ (Fig. 7). Its timing is consistent with widespread observations of Pliocene sedimentation-rate increases that have been attributed to climate change in which both the sediment flux and the mean grain size increase (Zhang *et al.*, 2001; Molnar, 2004). In contrast, at Taxi He a striking decrease in grain size occurs at the base of the second-order upward-coarsening cycle at ~4 Ma as accumulation rates increase (Fig. 10). We interpret this abrupt fining to be a response to accelerated subsidence and temporary retraction of the gravel front due to enhanced tectonic loading (Burbank, 1992). We suggest that the absence of a significantly increased flux of coarse sediment, despite an increased rate of sediment accumulation, is more consistent with tectonic, rather than climatic, forcing. Before 4 Ma, our data

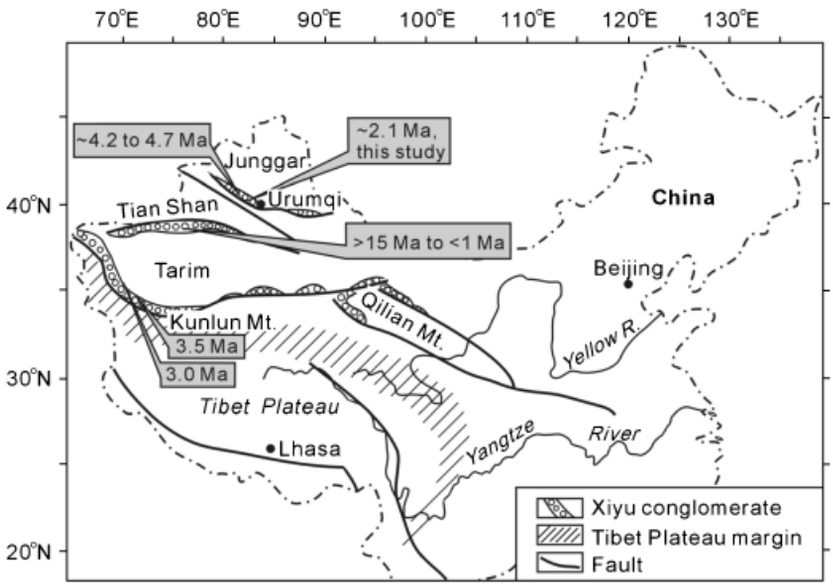

Fig. 15. Distribution of the foreland Xiyu conglomerate deposits in northwest China (after Liu *et al.*, 1996). The magnetostratigraphic ages of the basal Xiyu deposition indicate its diachronous nature. The age data are from Table 2.

Table 2. Magnetostratigraphic ages of the basal Xiyu conglomerates in northwest China

Studied area	Studied sections	Basal age of Xiyu Fm. (Ma)	References
Northern Chinese Tian Shan foreland	Kuitun He (west) section	4.7 ± 0.2 (reinterpreted)	Sun *et al.* (2007)
	Kuitun He (east) section	4.7 ± 0.2	Charreau *et al.* (2005)
	Dushanzi section	4.2 ± 0.2 (reinterpreted)	Sun *et al.* (2004)
	Taxi He section	~2.1	This study
Southwestern Chinese Tian Shan foreland	Ganhangou section	< 1.0	Chen *et al.* (2002)
	Boguzihe section	1.9	Chen *et al.* (2002)
	Northern Kashi foreland	15.5	Heermance *et al.* (2007)
	Middle Kashi foreland	8.6	Heermance *et al.* (2007)
	Southern Kashi foreland	1.9, 1.4, 0.7	Chen *et al.* (2007)
North piedmont of the Kunlun Mts.	Sanju section	3.0	Sun & Liu (2006)
	Yecheng section	3.5	Zheng *et al.*, 2000

indicate steady rates of sediment accumulation (Fig. 7). From this steadiness, we infer that, although folding had begun earlier in zone I (Qigu to Tuostai anticlines, Fig. 1b), initial stages of deformation and rock uplift had minimal impact on crustal thickness and tectonic loads because the uplifted foreland strata would have been readily eroded, such that little new topography or crustal thickening would result (Burbank & Beck, 1988; Molnar *et al.*, 1993; Burbank *et al.*, 1999; Sobel *et al.*, 2006). Only when the more erosion-resistant, pre-Jurassic bedrock emerged at the surface of the growing folds would significant thickening begin to drive enhanced foreland subsidence. Our data suggest that this emergence occurred at ~4 Ma.

Asynchronous Xiyu conglomerate deposits in northwest China

The conglomeratic Xiyu Formation is widely developed along both the northern and southern piedmonts of the Chinese Tian Shan (Liu *et al.*, 1996; Fig. 15). Further south it also is found on the northern piedmonts of the Kunlun Mountains and the Qilian Mountains (Fig. 15). This formation has been widely interpreted as marking an important tectonic and/or climatic event (Li *et al.*, 1979; Huang & Cheng, 1981; Liu *et al.*, 1996; Zheng *et al.*, 2000; Sun *et al.*, 2004, 2005a) and has commonly been viewed as a chronostratigraphic unit (Li *et al.*, 1979; Huang & Cheng, 1981). As demonstrated by several previous studies from the Tian Shan (Chen *et al.*, 2002; Charreau *et al.*, 2005; Heermance *et al.*, 2007), however, the onslaught of this facies is asynchronous. The magnetostratigraphic ages of the Xiyu conglomerate throughout northwest China (Table 2 and Fig. 15) unambiguously indicate its time-transgressive nature. In the piedmont subsidence zones on both sides of the Tian Shan, the basal Xiyu conglomerates range from middle Miocene (> 15 Ma) to middle Pleistocene (< 1 Ma) in age (Chen *et al.*, 2002, 2007; Sun *et al.*, 2004; Charreau *et al.*, 2005; Heermance *et al.*, 2007; this study), whereas farther south, basal ages range from ~3.5 to 3.0 Ma on the northern flank of the Kunlun Mts. (Zheng *et al.*, 2000; Sun & Liu, 2006). Such variations in age clearly indicate that the Xiyu conglomerate in northwest China should only be considered as a lithostratigraphic unit that lacks temporal implications beyond the local area for which its age has been independently defined.

CONCLUSION

Our paleomagnetic investigation provides a new, detailed chronology for the upper Cenozoic terrigenous sequence in the Tugulu anticline of the northern Tian Shan foreland. Our magnetostratigraphic correlation indicates that the ~1200-m-thick Taxi He section spans from ~8.1 to ~2.0 Ma. Although sediment-accumulation rates average ~200 m Myr^{-1} over this 6-Myr interval, they abruptly increase by >50% at ~4 Ma. We interpret this increase to result from accelerated subsidence that was, in turn, driven by enhanced rates of tectonic loading. Whereas slip on faults in the hinterland and within the proximal foreland undoubtedly began before 4 Ma, we speculate that continuing deformation brought more resistant rocks to the surface at this time, driving accelerated rates of surface uplift, crustal thickening, and tectonic loading. Initial growth of the Tugulu fold is interpreted from growth strata dated at ~6 Ma. Over 1 km of conglomerates dipping up to 45° overlie our dated section, suggesting that major topographic emergence of this fold occurred well after ~2 Ma. Based on this new magnetostratigraphy, the basal age of the Xiyu conglomerate in the Taxi He section is ~2.1 Ma: younger than the previous reported ages of 2.6 and 4.8 Ma for foreland folds about 130 km to the west. Whereas some previous studies interpreted the onset of massive conglomeratic deposition at diverse sites within the foreland as indicative of tectonic uplift of the Tian Shan at various times between 7 and 1 Ma, a synthesis of chronologic data for the Xiyu conglomerate clearly demonstrates its time-transgressive nature and reduces its utility for predicting time-specific tectonic events in the hinterland based on the site-specific age of foreland conglomerates. Balanced cross sections and inferred stratigraphic ages indicate net shortening of 1.5–10 km within the medial to distal northern Tian Shan foreland at rates of 0.2–1 mm yr^{-1} over the past 6–7 My. Although better age constraints are needed on structures in the proximal foreland, seismic reflection lines and previous work suggest that deformation began earlier in these more proximal sites. The subsequent northward migration of deformation drove the progradation of the coarsening-upward alluvial system that is widely preserved across the northern Tian Shan foreland. In the vicinity of the Taxi He section, the overarching, first-order depositional sequence comprises an initial shallow lacustrine environment that was succeeded by alluvial fan deposition after ~5.9 Ma. Enhanced understanding of the dynamics of the northern Tian Shan's depositional and tectonic evolution awaits more detailed and densely spaced chronostratigraphic studies.

ACKNOWLEDGEMENTS

Honghua Lu gives special appreciation to China Scholarship Council which supported him to study at University of California at Santa Barbara. We thank Dongjiang Sun, Supei Si, Hongzhuang Zhao and Mang Qian for their field assistance. We are especially grateful to Zhengyu Yang for the use of and assistance in the Paleomagnetic Laboratory of the Institute of Geomechanics, Chinese Academy of Geological Sciences in Beijing, and to Linfeng Shi, Xiaodi Zhou, and Jianli Fu for their assistance in the lab. This paper benefited from discussions with Zhengkai Xia, Mingda Ren, Jingchun Yang and Joseph Goode. We especially thank Richard Lease for his assistance in the analysis of the paleomagnetic data. Thoughtful and thorough reviews by G. Dupon-Nivet, J. Charreau, another anonymous reviewer, and editor P. van der Beek profoundly improved this manuscript. This study was financially supported by National Natural Science Foundation of China (Grant 40571013) and by the US National Science Foundation (EAR 0230403).

REFERENCES

Abdrakhmatov, K.Y., Aldazhanov, S.A., Hager, B.H., Hamburger, M.W., Herring, T.A., Kalabaev, K.B., Makarov, V.I., Molnar, P., Panasyuk, S.V., Prilepin, M.T., Reilinger, R.E., Sadybakasov, I.S., Souter, B.J., Trapeznikov, Y.A., Tsurkov, V.Y. & Zubovich, A.V. (1996) Relatively recent construction of the Tien Shan inferred from GPS measurements of present-day crustal deformation rates. *Nature*, **384**, 450–453, doi: 10.1038/384450a0.

Allen, M.B., Windley, B.F., Zhang, C. & Guo, J.H. (1993) Evolution of the Turfan Basin, Chinese Central Asia. *Tectonics*, **12**(4), 889–896.

Avouac, J.-P. & Tapponnier, P. (1993) Kinematic model of active deformation in central Asia. *Geophys. Res. Lett.*, **20**(10), 895–898.

Avouac, J.-P., Tapponnier, P., Bai, P., You, M. & Wang, G. (1993) Active thrusting and folding along the northern Tien Shan and late Cenozoic rotation of the Tarim relative to Dzungaria and Kazakhstan. *J. Geophys. Res.*, **98**(B4), 6755–6804.

Blair, T.C. & McPherson, J.G. (1994) Alluvial fans and their natural distinction from rivers based on morphology, hydraulic processes, sedimentary processes and facies assemblages. *J. Sedim. Res.*, **64**(3a), 450–489.

Bullen, M.E., Burbank, D.W., Garver, J. & Abdrakhmatov, K.Y. (2001) Late Cenozoic tectonic evolution of the northwestern Tien Shan: new age estimates for the initiation of mountain building. *Geol. Soc. Am. Bull.*, **113**(12), 1544–1559.

Bullen, M.E., Burbank, D.W. & Garver, J. (2003) Building the northern Tien Shan: integrated thermal, structural, and topographic constraints. *J. Geol.*, **111**, 149–165.

Burbank, D.W. (1992) Causes of recent Himalayan uplift deduced from deposited patterns in the Ganges basin. *Nature*, **357**, 680–683, doi: 10.1038/357680a0.

Burbank, D.W. & Beck, R.A. (1988) Rapid, long-term rates of denudation. *Geology*, **19**, 1169–1172.

Burbank, D.W., Beck, R.A., Raynolds, R.G.H., Hobbs, R. & Tahirkheli, R.A.K. (1988) Thrusting and gravel progradation in foreland basins: a test of post-thrusting gravel dispersal. *Geology*, **16**(2), 1143–1146.

Burbank, D.W., McLean, J.K., Bullen, M., Abdrakhmatov, K.Y. & Miller, M.M. (1999) Partitioning of intermontane basins by thrust-related folding, Tien Shan, Kyrgyzstan. *Basin Res.*, **11**(1), 75–92.

Burbank, D.W., Meigs, A. & Brozovic, N. (1996) Interactions of growing folds and coeval depositional systems. *Basin Res.*, **8**, 199–223.

Burchfiel, B.C., Brown, E.T., Deng, Q., Feng, X., Li, J., Molnar, P., Shi, J., Wu, Z. & You, H. (1999) Crustal shortening on the margins of the Tien Shan, Xinjiang, China. *Int. Geol. Rev.*, **41**(8), 665–700.

Bureau of Geological and Mineral Resources of the Xinjiang Uygur Autonomous Region. (1993) *Regional Geology of Xinjiang Uygur Antonomous Region*. Geology Press, Beijing, 841pp (in Chinese).

Burtman, V.S. (1975) Structural geology of the Variscan Tien Shan. *Am. J. Sci.*, **280**, 725–744.

Butler, R.L. (1992) *Paleomagnetism*. Blackwell Scientific Publications, Cambridge, MA.

Carroll, A.R., Graham, S.A., Hendrix, M.S., Ying, D. & Zhou, D. (1995) Late Paleozoic tectonic amalgamation of northwestern China: sedimentary record of the northern Tarim, northwestern Turpan, and southern Junggar basins. *Geol. Soc. Am. Bull.*, **107**, 571–594.

Charreau, J., Avouac, J.-P., Chen, Y., Dominguez, S. & Gilder, S. (2008b) Miocene to present kinematics of fault-bend folding across the Huerguosi anticline, northern Tianshan (China), derived from structural, seismic, and magnetostratigraphic data. *Geology*, **36**(11), 871–874.

Charreau, J., Chen, Y., Gilder, S., Dominguez, S., Avouac, J.-P., Sen, S., Sun, D.J., Li, Y.A. & Wang, W.M. (2005) Magnetostratigraphy and rock magnetism of the Neogene Kuitun He section (northwest China): implications for Late Cenozoic uplift of the Tianshan mountains. *Earth Planet. Sci. Lett.*, **230**, 177–192.

Charreau, J., Gilder, S., Chen, Y., Dominguez, S., Avouac, J.-P., Sen, S., Jolivet, M., Li, Y.A. & Wang, W.M. (2006) Magnetostratigraphy of the Yaha section, Tarim Basin (China): 11 Ma acceleration in erosion and uplift of the Tian Shan Mountains. *Geology*, **34**(3), 181–184.

Charreau, J., Sun, J., Chen, Y., Gilder, S., Huang, B. & Wang, Q. (2008a) Addendum to "Late Cenozoic magnetochronology and paleoenvironmental changes in the northern foreland basin of the Tian Shan Mountains" by Jimin Sun, Qinghai Xu, and Baochun Huang. *J. Geophys. Res.*, **113**, B06103, doi: 10.1029/2007JB005489.

Chen, J., Burbank, D.W., Scharer, K.M., Sobel, E., Jinhui, Y., Rubin, C. & Ruibin, Z. (2002) Magnetochronology of the Upper Cenozoic strata in the Southern Chinese Tian Shan: rates of Pleistocene folding and thrusting. *Earth Planet. Sci. Lett.*, **195**, 113–130.

Chen, J., Heermance, R., Burbank, D.W., Scharer, K.M., Miao, J.J. & Wang, C.S. (2007) Quantification of growth and lateral propagation of the Kashi anticline, southwest Chinese Tian Shan. *J. Geophys. Res.*, **112**, doi: 10.1029/2006JB004345.

Colombo, F. (1994) Normal and reverse unroofing sequences in syntectonic conglomerates as evidence of progressive basinward deformation. *Geology*, **22**(3), 235–238.

Daëron, M., Avouac, J.-P. & Charreau, J. (2007) Modeling the shortening history of a fault tip fold using structural and geomorphic records of deformation. *J. Geophys. Res.*, **112**, B03S13, doi: 10.1029/2006JB004460.

DeCelles, P.G. (1994) Late Cretaceous-Paleocene synorogenic sedimentation and kinematic history of the Sevier thrust belt, northeast Utah and southwest Wyoming. *Geol. Soc. Am. Bull.*, **106**, 32–56.

DeCelles, P.G., Gehrels, G.E., Quade, J. & OJHA, P. (1998) Eocene-early Miocene foreland basin development and the history of Himalayan thrusting, western and central Nepal. *Tectonics*, **17**(5), 741–765.

DeCelles, P.G. & Giles, K.A. (1996) Foreland basin systems. *Basin Res.*, **8**, 105–123.

DeCelles, P.G., Gray, M.B., Ridgway, K.D., Cole, R.B., Pivnik, D.A., Pequera, N. & Srivastava, P. (1991) Controls on synorogenic alluvial-fan architecture, Beartooth Conglomerate (Palaeocene), Wyoming and Montana. *Sedimentology*, **38**, 567–590.

Deng, Q.D., Feng, X.Y., You, H.C., Zhang, P.Z., Zhang, Y., Li, J., Wu, Z.M., Xu, X.W., Yang, X.P. & Zhang, H.W. (1991) The characteristic of deformation and mechanism of Dushanzi- Anjihai active reverse fault-fold zone in the northern flank of the Tian Shan Mountains. In: *Research of Active Fault (I)* (Ed. by Editing Committee of the Research of Active Fault) pp. 17–36. Seismology Press, Beijing (in Chinese, English abstract).

Deng, Q.D., Feng, X.Y., Zhang, P.Z., Xu, X.W., Yang, X.P., Peng, S.Z. & Li, J. (2000) *Active Tectonics of the Tian Shan Mountains*. Seismology Press, Beijing, 399pp (in Chinese).

Dumitru, T.A., Zhou, D., Chang, E.Z., Graham, S.A., Hendrix, M.S., Sobel, E.R. & Carroll, A.R. (2001) Uplift, exhumation, and deformation in the Chinese Tian Shan. In: *Paleozoic and Mesozoic Tectonic Evolution of Central and Eastern Asia: From Continental Assembly to Intracontinental Deformation (194)* (Ed. by M.S. Hendrix & G.A. Davis), *Geol. Soc. Am. Memoir*, 71–99.

Dupont-Nivet, G., Krijgsman, W., Langereis, C.G., Abels, H.A., Dai, S. & Fang, X. (2007) Tibetan plateau aridification linked to global cooling at the Eocene-Oligocene transition. *Nature*, **445**, 635–638.

Editing Committee of the Stratigraphy of China. (1999) *Stratigraphy in China (Teritary)*. Geology Press, Beijing, 163pp (in Chinese).

Fu, B., Lin, A., Kano, K.-I., Maruyama, T., Guo, J. & Abdrakhmatov, K.Y. (2003) Quaternary folding of the eastern Tian Shan, northern China. *Tectonophysics*, **369**, 79–101.

Gansser, A. (1981) The geodynamic history of the Himalaya. In: *Zagros, Hindu Kush, Himalaya Geodynamic Evolution (3)* (Ed. by H.K. Gupta & F.M. Delany), pp. 111–121. American Geophysical Union, Washington, DC.

Heermance, R.V., Chen, J., Burbank, D.W. & Wang, C.S. (2007) Chronology and tectonic controls of Late Tertiary deposition in the southwestern Tian Shan foreland, NW China. *Basin Res.*, **19**, 599–632.

Heller, P.L., Angevine, C.L., Winslow, N.S. & Paola, C. (1988) Two-phase stratrgraphic model of foreland-basin sequences. *Geology*, **16**, 501–504.

Heller, P.L. & Paola, C. (1992) The large-scale dynamics of grain-size variation in alluvial basins, 2: application to syntectonic conglomerate. *Basin Res.*, **4**, 91–102.

Hendrix, M.S., Dumitru, T.A. & Graham, S.A. (1994) Late Oligocene-early Miocene unroofing in the Chinese Tian shan: an early effect of the India-Asia collision. *Geology*, **22**, 487–490.

Hendrix, M.S., Graham, A.S., Carroll, A.R., Sobel, E.R., McKnight, C.L., Schulein, B.J. & Wang, Z. (1992) Sedimentary record and climatic implications of deformation in the Tian Shan: evidence from Mesozoic strata of the north Tarim, south Junggar, and Turpan Basins, northwest China. *Geol. Soc. Am. Bull.*, **104**, 53–79.

Huang, B.C., Piper, J.D.A., Peng, S.T., Liu, T., Li, Z., Wang, Q.C. & Zhu, R.X. (2006) Magnetostragraphic study of the Kuche Depression, Tarim Basin, and Cenozic uplift of the Tian Shan Range, Western China. *Earth Planet. Sci. Lett.*, **251**, 346–364.

Huang, T.K. & Cheng, B.W. (1981) Pliocene-Quaternary molasse deposits in the Tethys-Himalayan tectonic domain and its relation with the Indian Plate motion. In: *Scientific Papers on Geology for International Exchange (I)* (Ed. by Editing Group of Book and News in Ministry of Geology) pp. 1–14. Geology Press, Beijing (in Chinese).

Jones, M.A., Heller, P.L., Roca, E., Garcés, M. & Cabrera, L. (2004) Time lag of syntectonic sedimentation across an alluvial basin: theory and example from the Ebro Basin, Spain. *Basin Res.*, **16**, 467–488.

Jordan, T.E., Flemings, P.B. & Beers, J.A. (1988) Dating thrust-fault activity by use of foreland-basin strata. In: *New Perspectives in Basin Analysis* (Ed. by K.L. Kleinspehn & C. Paola), pp. 307–330. Springer-Verlag, New York.

Kirschvink, J.L. (1980) The Least-Squares line and plane and analysis of paleomagnetic data. *Geophys. J. Int.*, **62**(3), 699–718, doi: 10.1111/j.1365-246X.1980.tb02601.x.

Li, J.J., Wen, S.X., Zhang, Q.S., Wang, F.B., Zheng, B.X. & Li, B.Y. (1979) A discussion on the period, amplitude and type of the uplift of the Qinghai-Xizang Plateau. *Sci. Sinica (Series A)*, **22**(11), 1314–1328 (in Chinese, English abstract).

Liu, T.S., Ding, M.G. & Derbyshire, E. (1996) Gravel deposits on the margins of the Qinghai-Xizang plateau, and their environmental significance. *Palaeogeogr. Palaeoclimatol. Palaeoecol.*, **120**, 159–170.

Lü, H., Xia, Z., Jiang, B., Ren, M. & Li, Y. (2006) Application of mathematical geology methods to analysis of the sedimentary facies of sandstone reservoir: an example of the reservoir of the Neogene in Huatugou Oilfield, Qaidam Basin. *Acta Sci. Nat. Univ. Pekinensis*, **42**(4), 462–469 (in Chinese, English abstract).

Lourens, L., Hilgen, F., Shackelton, N.J., Laskar, J. & Wilson, D. (2004) The Neogene Period. In: *A Geologic Time Scale* (Ed. by F.M. Gradstein, J.G. Ogg & A.G. Smith), pp. 409–440. Cambridge University Press, Cambridge.

Magee, J.W., Bowler, J.M., Miller, G.H. & Williams, D.L.G. (1995) Stratigraphy, sedimentology, chronology and palaeohydrology of Quaternary lacustrine deposits at Madigan Gulf, Lake Eyre, south Australia. *Palaeogeogr. Palaeoclimatol. Palaeoecol.*, **113**, 3–42.

McElhinny, M.W. (1964) Statistical significance of the fold test in paleomagnetism. *Geophys. J. Int.*, **8**(3), 338–340, doi: 10.1111/j.1365-246X.1964.tb06300.x.

McFadden, P.L. & McElhinny, M.W. (1990) Classification of the reversal test in palaeomagnetism. *Geophys. J. Int.*, **103**, 725–729.

Métivier, F. & Gaudemer, Y. (1997) Mass transfer between eastern Tien Shan and adjacent basins (central Asia): constraints on regional tectonics. *Geophys. J. Int.*, **128**, 1–17.

Miall, A.D. (1978) Lithofacies types and vertical profile models in braided river deposits: a summary. In: *Fluvial Sedimentology* **5** (Ed. by A.D. Miall), *Memoir, Canad. Soc. Petrol. Geol.,* 597–604.

Molnar, P. (2001) Climate change, flooding in arid environments, and erosion rates. *Geology*, **29**(12), 1071–1074.

Molnar, P. (2004) Late Cenozoic increase in accumulation rates of terrestrial sediment: how might climate change have affected erosion rates? *Annu. Rev. Earth Planet. Sci.*, **32**, 67–89.

Molnar, P., Brown, E.T., Burchfiel, B.C., Deng, Q.D., Feng, .X.Y., Li, J., Raisbeck, G.M., Shi, J.B., Wu, Z.M., Yiou, F. & You, H.C. (1994) Quaternary climate change and the formation of river terraces across growing anticlines on the north flank of the Tien Shan, China. *J. Geol.*, **102**, 583–602.

Molnar, P., England, P. & Martinod, J. (1993) Mantle dynamics, uplift of the Tibetan Plateau, and the Indian monsoon. *Rev. Geophys.*, **31**(4), 357–396.

Molnar, P. & Tapponnier, P. (1975) Cenozoic tectonics of Asia: effects of a continental collision. *Science*, **189**, 419–426.

Nemec, W. & Steel, R.J. (1984) Alluvial and coastal conglomerates: their significant features and some comments on gravelly mass-flow deposits. In: *Sedimentology of Gravels and Conglomerates (10)* (Ed. by E.H. Koster & R.J. Steel), pp. 1–32. Canadian Society of Petroleum Geologists, Calgary.

Ortí, F., Rosell, L. & Anadón, P. (2003) Deep to shallow lacustrine evaporites in the Libros gypsum (Southern Teruel Basin, Miocene, Ne Spain): an occurrence of Pelletal Gypsum Rhythmites. *Sedimentology*, **50**(2), 361–386.

Oskin, M. & Burbank, D.W. (2005) Alpine landscape evolution dominated by cirque retreat. *Geology*, **33**, 933–936.

Oskin, M. & Burbank, D.W. (2007) Transient landscape evolution of basement-cored uplifts: example of the Kyrgyz Range, Tian Shan. *J. Geophys. Res.*, **112**, F03S03, doi: 10.1029/2006JF000563.

Parès, J.M., Van Der Voo, R., Downs, W.R., Yan, M. & Fang, X. (2003) Northeastward growth of the Tibetan Plateau: magnetostratigraphic insights from the Guide basin. *J. Geophys. Res.*, **108**(B8), 1–11.

Patriat, P.A. & Achache, J. (1984) India-Eurasia collision chronology has implications for crustal shortening and driving mechanisms of plates. *Nature*, **311**(5987), 615–621.

Peng, X.L. (1975) Cenozoic vertebrate localities and horizon of Junggar Basin, Xinjiang. *Vérteb. PalAs.*, **13**(3), 185–189 (in Chinese, English abstract).

Ren, M.D. & Wang, N.L. (1985) *An Introduction to Modern Sedimentary Environments*. Science Press, Beijing, 231pp (in Chinese).

Rust, B.R. (1978) Depositional models fro braided alluvium. In: *Fluvial Sedimentology (5)* (Ed. by A.D. Miall), *Canad. Soc. Petrol. Geol., Memoir* 605–625.

Sobel, E.R., Oskin, M., Burbank, D.W. & Mikolaichuk, A. (2006) Exhumation of basement-cored uplifts: example of the Kyrgyz Range quantified with apatite fission track thermochronology. *Tectonics*, **25**, doi: 10.1029/2005TC001809.

Song, C.H., Fang, X.M., Li, J.J., Gao, J.P., Zhao, Z.J. & Fan, M.J. (2001) Tectonic uplift and sedimentary evolution of Jiuxi Basin in the northern margin of Tibetan Plateau since 13 Ma. *Sci. China (Series D)*, **44**(Suppl), 192–202.

Sun, J.M. & Liu, T.S. (2006) The age of the Taklimakan Desert. *Science*, **312**, 1621.

Sun, J.M., Xu, Q.H. & Huang, B.C. (2007) Late Cenozoic magnetochronology and paleoenvironmental changes in the northern foreland basin of the Tian Shan Mountains. *J. Geophys. Res.*, **112**, B04107, doi: 10.1029/2006JB004653.

Sun, J.M., Zhu, R.X. & An, Z.S. (2005a) Tectonic uplift in the northern Tibetan Plateau since 13.7 Ma ago inferred from molasses deposits along the Altyn Tagh Fault. *Earth Planet. Sci. Lett.*, **235**, 641–653.

Sun, J.M., Zhu, R.X. & Bowler, J. (2004) Timing of the Tianshan Mountains uplift constrained by magnetostratigraphic analysis of molasses deposits. *Earth Planet. Sci. Lett.*, **219**, 239–253.

Sun, Z.M., Yang, Z.Y., Pei, J.L., Ge, X.H., Wang, X.S., Yang, T.S., Li, W.M. & Yuan, S.H. (2005b) Magnetostratigraphy of Paleogene sediments from northern Qaidam Basin, China: implications for tectonic uplift and block rotation in northern Tibetan plateau. *Earth Planet. Sci. Lett.*, **237**, 635–646.

Suppe, J., Chou, G.T. & Hook, S.C. (1992) Rates of folding and faulting determined from growth strata. In: *Thrust Tectonics* (Ed. by K.R. McClay), pp. 105–121. Chapman & Hall, Suffolk.

Talling, P.J. & Burbank, D.W. (1993) Assessment of uncertainties in magnetostratigraphic dating of sedimentary strata. In:

Applications of Paleomagnetism to Sedimentary Geology (49) (Ed. by D.M. Aissaoui, D.F. McNeil & N.F. Hurley), *SEPM (Soc. Sediment. Geol.) Spec. Publ.*, 59–69.

Tapponnier, P. & Molnar, P. (1979) Active faulting and Cenozoic tectonics of the Tien Shan, Mongolia, and Baykal regions. *J. Geophys. Res.*, **84**, 3425–3459.

Tapponnier, P., Zhiqin, X., Roger, F., Meyer, B., Arnaud, N., Wittlinger, G. & Jingsui, Y. (2001) Oblique stepwise rise and growth of the Tibetan Plateau. *Science*, **394**, 1671–1677.

Tucker, G.E. & Slingerland, R. (1996) Predicting sediment flux from fold and thrust belts. *Basin Res.*, **8**, 329–349.

Windley, B.F., Allen, M.B., Zhang, C., Zhao, Z.Y. & Wang, G.R. (1990) Paleozoic accretion and Cenozoic redeformation of the Chinese Tien Shan Range, Central Asia. *Geology*, **18**(2), 128–131.

Xu, C.M., He, X.S., Wu, X.Z. & Yao, X.Y. (1992) Structure analysis and petroleum exploration prospect of Tostai area in Juggar Basin. *Xinjiang Petrol. Geol.*, **13**(3), 197–205 (in Chinese, English abstract).

Yang, X.P., Deng, Q.D. & Feng, X.Y. (1996) Research on geometry, kinematics of Tugulu active reverse fault-fold in the northern flank of the Tian Shan Mountains. In: *Research of Active Fault (V)* (Ed. by Editing Committee of the Research of Active Fault), pp. 42–53. Seismology Press, Beijing (in Chinese, English abstract).

Yang, Y. & Liu, M. (2002) Cenozoic deformation of the Tarim plate and the implications for mountain building in the Tibetan Plateau and the Tian Shan. *Tectonics*, **21**(6), 1059, doi: 10.1029/2001TC001300.

Zhang, P.Z., Deng, Q.D., Xu, X.W., Wu, Z.M., Yang, X.P., Feng, X.Y., Li, J., Chen, W., Zhao, R.B. & Tang, W. (1994) Tectonic deformation, crustal shortening, and slip rate estimation along the Manas reverse fault-fold zone in the northern flank of the Tian Shan Mountains. In: *Research of Active Fault (III)* (Ed. by Editing of Committee of the Research of Active Fault), pp. 18–32. Seismology Press, Beijing (in Chinese, English abstract).

Zhang, P.Z., Molnar, P. & Downs, W.R. (2001) Increased sedimentation rates and grain sizes 2–4 Myr ago due to the influence of climate change on erosion rates. *Nature*, **410**, 891–897.

Zheng, H.B., Powell, C.M., An, Z.S., Zhou, J. & Dong, G.R. (2000) Pliocene uplift of the northern Tibetan Plateau. *Geology*, **28**(8), 715–718.

Manuscript received 9 July 2008; Manuscript accepted 5 March 2009.